CELL BIOLOGY

MARK3-mediated phosphorylation of ARHGEF2 couples microtubules to the actin cytoskeleton to establish cell polarity

María-José Sandí,[1] Christopher B. Marshall,[1]* Marc Balan,[1,2]* Étienne Coyaud,[1] Ming Zhou,[3] Daniel M. Monson,[3] Noboru Ishiyama,[1] Arun A. Chandrakumar,[1,2] José La Rose,[1] Amber L. Couzens,[4] Anne-Claude Gingras,[4,5] Brian Raught,[1,2] Wei Xu,[6,7] Mitsuhiko Ikura,[1,2] Deborah K. Morrison,[3] Robert Rottapel[1,2,8,9,10†]

The PAR-1–MARK pathway controls cell polarity through the phosphorylation of microtubule-associated proteins. Rho-Rac guanine nucleotide exchange factor 2 (ARHGEF2), which activates Ras homolog family member A (RHOA), is anchored to the microtubule network and sequestered in an inhibited state through binding to dynein light chain Tctex-1 type 1 (DYNLT1). We showed in mammalian cells that liver kinase B1 (LKB1) activated the microtubule affinity-regulating kinase 3 (MARK3), which in turn phosphorylated ARHGEF2 at Ser[151]. This modification disrupted the interaction between ARHGEF2 and DYNLT1 by generating a 14-3-3 binding site in ARHGEF2, thus causing ARHGEF2 to dissociate from microtubules. Phosphorylation of ARHGEF2 by MARK3 stimulated RHOA activation and the formation of stress fibers and focal adhesions, and was required for organized cellular architecture in three-dimensional culture. Protein phosphatase 2A (PP2A) dephosphorylated Ser[151] in ARHGEF2 to restore the inhibited state. Thus, we have identified a regulatory switch controlled by MARK3 that couples microtubules to the actin cytoskeleton to establish epithelial cell polarity through ARHGEF2.

INTRODUCTION

Control of cell polarity is essential for the establishment of multicellular tissues in metazoans. Genetic studies in the nematode *Caenorhabditis elegans* have identified a set of six *partition-defective* or *PAR* genes that participate in the polarity program during embryonic development and are conserved in mammals (*1*–*4*). PAR-1 is required for axis formation in oogenesis and establishment of oocytes in the fruit fly *Drosophila melanogaster*, both of which are processes associated with microtubule dynamics and stability (*5*). Mammals have four PAR-1 orthologs comprising the family of microtubule affinity-regulating kinases (MARKs), which are related to adenosine 5′-monophosphate–activated protein kinase (AMPK). The MARK family comprises four members: PAR-1a (also known as MARK3 or C-TAK), PAR-1b (also known as MARK2 or EMK), PAR-1c (also known as MARK1), and PAR-1d (also known as MARK4 or MARKL1). MARKs regulate cell polarity (*3*) and trigger microtubule instability by phosphorylating microtubule-associated proteins (MAPs), causing their rapid detachment from microtubules (*6*, *7*). The best-characterized family member, MARK2, modulates the growth of axonal projections in hippocampal neurons (*8*) and contributes to the formation of neurites in neuroblastoma cells (*9*) by phosphorylating the MAP tau (MAPT; also known as TAU). This phosphorylation event modulates microtubule plasticity, which is required for neuronal polarity and the growth of neurites (*8*, *9*). MARK2 also phosphorylates Rab11 family-interacting protein 2 (FIP2), which regulates lumen polarity (*10*) and the activity of catenin delta 1 (CTNND1; also known as catenin p120) at the junctional complexes (*11*). Loss of function of MARK2, MARK3, or MARK4 in mice leads to metabolic defects, including increased metabolic rate, decreased adiposity, defective gluconeogenesis, and insulin hypersensitivity (*12*–*14*). MARK2 and MARK3 can compensate for one another during embryogenesis; however, compound homozygous knockout of both is embryonic lethal (*12*, *15*), whereas loss of three of four alleles causes defects in the development of the glomerular and proximal tubules of the kidneys (*16*). All four MARKs are targets of the *Helicobacter pylori* virulence factor CagA, which disrupts tight junctions and polarity in epithelial cell lines (*17*). Other MAPs that are MARK substrates and that direct cell polarity have yet to be identified (*18*–*22*).

The Ras homolog family member A (RHOA) guanine nucleotide exchange factor ARHGEF2 has been implicated in various cellular processes involving the establishment of cell polarity, including epithelial tight junction formation (*23*), proximal tubule paracellular permeability (*24*), and endothelial permeability (*25*). We have described a RHOA-independent requirement of ARHGEF2 in rat sarcoma–mediated transformation (*26*). ARHGEF2 is sequestered in an inhibited state on the microtubule array, where it is tethered by the dynein motor light chain DYNLT1 (*27*, *28*), and phosphorylated by PAK1 [p21 (RAC1)–activated kinase 1] or PKA (protein kinase A) on the C-terminal negative regulatory site Ser[886] (*28*, *29*). Phosphorylation at Ser[886] creates a binding site for 14-3-3 proteins, which hold ARHGEF2 in a catalytically inactive configuration (*28*). ARHGEF2 can be activated by disassembly of the microtubule array using pharmacologic agents or by the physiologic ligands lysophosphatidic acid and thrombin (*30*).

To elucidate the detailed mechanisms by which ARHGEF2 is positively regulated and coupled to the cell polarity program, we sought to systematically determine the ARHGEF2 interaction network using a proteomic approach. We identified MARK3 as a positive regulator of

[1]Princess Margaret Cancer Centre, University Health Network, 101 College Street, Princess Margaret Cancer Research Tower, Toronto, Ontario M5G 1L7, Canada. [2]Department of Medical Biophysics, University of Toronto, 1 King's College Circle, Toronto, Ontario M5S 1A8, Canada. [3]Center for Cancer Research, National Cancer Institute at Frederick, P.O. Box B, Frederick, MD 21702, USA. [4]Lunenfeld-Tanenbaum Research Institute, Mount Sinai Hospital, 600 University Avenue, Toronto, Ontario M5G 1X5, Canada. [5]Department of Molecular Genetics, University of Toronto, Toronto, Ontario M5S 1A8, Canada. [6]Dalla Lana School of Public Health, University of Toronto, Toronto, Ontario, Canada. [7]Department of Biostatistics, Princess Margaret Cancer Centre, Toronto, Ontario, Canada. [8]Department of Medicine, University of Toronto, Toronto, Ontario M5S 1A8, Canada. [9]Department of Immunology, University of Toronto, Toronto, Ontario M5S 1A8, Canada. [10]Division of Rheumatology, St. Michael's Hospital, 30 Bond Street, Toronto, Ontario M5B 1W8, Canada.
*These authors contributed equally to this work.
†Corresponding author. Email: rottapel@uhnresearch.ca

ARHGEF2. MARK3 phosphorylated ARHGEF2 on Ser^{151}, which we demonstrated using x-ray crystallographic structure determination, is contained within the DYNLT1-binding region. We showed that the sequence encompassing Ser^{151} is conserved across species and is a functional 14-3-3 binding site. When 14-3-3 bound to phospho-Ser^{151}, ARHGEF2 was displaced from the dynein motor complex, thereby promoting a catalytically active ARHGEF2 pool that was dissociated from microtubules. Binding of 14-3-3 to phospho-Ser^{151}–ARHGEF2 induced its relocalization to the plasma membrane and cytoplasmic compartments, where it activated RHOA to promote the induction of stress fibers and focal adhesions, whereas Ser^{151} phosphorylation was antagonized by protein phosphatase 2A (PP2A) phosphatase. We identified ARHGEF2 as a MARK3 substrate activated by a phospho-switch controlling its association with DYNLT1 and showed that this phosphorylation event was required for the formation of polarized spheroid structures.

RESULTS

ARHGEF2 interaction network comprises proteins associated with microtubules or cell division processes

To identify new ARHGEF2 interactors, we used proximity-dependent biotin identification (BioID) (*31*) by stably expressing Flag-tagged bifunctional ligase-repressor (BirA*) fused to ARHGEF2 in 293 Flp-In T-REx cells, followed by affinity purification and mass spectrometry (MS) (*32*). We confirmed six previously known ARHGEF2-interacting proteins, including p21 (RAC1)–activated kinase 4 (PAK4), MARK2, centrosomal protein 170 (CEP170) (*33*–*36*), and the protein phosphatase 6 catalytic subunit (PPP6C), regulatory subunit 1 (PPP6R1), and the ankyrin repeat domain 28 (ANKRD28) subunit (Fig. 1A, fig. S1A, and table S1) (*37*). Gene ontology (GO) analysis and a survey of the literature revealed that many of the ARHGEF2 interactors were associated with (i) microtubule organization and regulation, (ii) vesicle-mediated transport (*38*), (iii) mitotic cell cycle processes, and (iv) cell polarity (fig. S1B and tables S2 and S3). An ARHGEF2 interactor of particular interest was MARK3 (also known as C-TAK1). MARK3 associates with and phosphorylates cell division cycle 25C (CDC25C) (*39*) and many other substrates, including protein tyrosine phosphatase H1 (PTPH1), kinase suppressor of Ras1 (KSR1), and plakophilin2 (PKP2) (*40*). We further investigated the function of the MARK3-ARHGEF2 complex because these proteins have a common role in promoting microtubule dynamics.

MARK3 interacts with and phosphorylates ARHGEF2 and other MAPs

To understand the potential role of MARK3 and ARHGEF2 signaling networks, we next sought to elucidate the protein interaction network of MARK3. Pyo-tagged MARK3 protein complexes were affinity-purified from 293T cells and identified using MS. Known MARK3 substrates including KSR1 and PTPH1 were detected in this analysis in addition to new MARK3-interacting peptides (Fig. 1B and table S4). Of these, cytoplasmic linker-associated proteins 1 and 2 (CLASP1 and CLASP2) and ARHGEF2 are known microtubule-binding proteins. To confirm the interaction of MARK3 with CLASP1, CLASP2, and ARHGEF2, coimmunoprecipitation assays were performed using constructs expressing Pyo-tagged MARK3 or connector enhancer of kinase suppressor of Ras 1[Pyo-CNK1, a protein scaffold not known to bind to any of the putative MARK3 substrates (*41*)]. CLASP1, CLASP2, and ARHGEF2 were detected in immunoprecipitates of MARK3 but not of CNK1 (Fig. 1C). MARK3 was identified in ARHGEF2 immunoprecipitates from 293T cells, confirming an interaction between the endogenous proteins (Fig. 1D). Next, we examined whether these proteins were MARK3 substrates by performing in vitro [γ-^{32}P]ATP (adenosine 5′-triphosphate) kinase assays with immune complexes. CLASP1, CLASP2, ARHGEF2, or the N-terminal domain of KSR1 was isolated from transfected Cos-7 cells under stringent lysis conditions. MARK3^{WT} exhibited autokinase activity and phosphorylated the positive control substrate KSR1, whereas MARK3^{KD} did not. In addition, CLASP1, CLASP2, and ARHGEF2 were strongly phosphorylated by MARK3^{WT} but not by MARK3^{KD} (Fig. 1E). These data demonstrated that CLASP1, CLASP2, and ARHGEF2 are MARK3 substrates, and all contained MARK3 consensus phosphorylation motifs Φ^axRxxS*ΦPxxΦ^a or Φ^axR/KxxS*xxxΦ^a (where S* is the site phosphorylated, x is any amino acid, Φ^a is a hydrophobic residue with an aliphatic side chain, and Φ is any hydrophobic amino acid) (*40*, *42*, *43*) at sites corresponding to CLASP1 Ser^{600} and Ser^{1162}, and CLASP2 Ser^{370} and ARHGEF2 Ser^{151} (Fig. 1F).

MARK3 phosphorylates ARHGEF2 on Ser^{151} and creates a 14-3-3 binding site

We mapped the MARK3 binding site on ARHGEF2 using a series of Flag-tagged ARHGEF2 fragments and detected MARK3 only in immunoprecipitates containing the N-terminal portion ARHGEF2. Residues 1 to 243 were necessary for interaction with MARK3, and the addition of the Dbl homology (DH) and pleckstrin homology (PH) domains each contributed to promote maximal binding, although an isolated DH-PH domain failed to bind MARK3 (Fig. 2A).

To determine the sites on ARHGEF2 phosphorylated by MARK3, phosphopeptide mapping analysis was performed on the phosphopeptides generated in vitro. The major phosphorylation site was contained within a phosphopeptide that eluted in fractions 37 and 38. Edman degradation and phosphoamino acid analysis revealed that Ser^{151} was the residue phosphorylated in this tryptic fragment. When a similar analysis was performed using an ARHGEF2 mutant lacking Ser^{151} (ARHGEF2^{S151A}), the phosphopeptide eluting in fractions 37 and 38 was nearly abolished (Fig. 2B). Phosphopeptide analysis of in vivo ^{32}P-labeled wild-type ARHGEF2 further confirmed that ARHGEF2 Ser^{151} was phosphorylated in intact cells (Fig. 2C).

To validate that ARHGEF2 was a substrate of MARK3, we examined whether MARK3 could phosphorylate ARHGEF2 Ser^{151} in vitro if key residues in the MARK3 consensus phosphorylation motif were mutated. On the basis of the radioactivity incorporated into Ser^{151}, loss of the hydrophobic residues at positions −5 and +4 and loss of the lysine residue at −3 each severely reduced MARK3 phosphorylation of Ser^{151} (Fig. 2D). These data confirmed that ARHGEF2 is a bona fide substrate of MARK3. Whereas ARHGEF2 orthologs exhibit 67% sequence identity overall (fig. S2), the MARK3 consensus motif residues are completely conserved among vertebrates, including reptiles, amphibians, fishes, and mammals, suggesting an important functional role of this site (Fig. 2E).

MARK3 phosphorylation of peptide sequences in other substrates frequently creates 14-3-3 binding sites. The ARHGEF2 fragment comprising residues 1 to 243 coimmunoprecipitated with endogenous 14-3-3 (Fig. 2A). To characterize the interaction of ARHGEF2 with 14-3-3 in vitro, we analyzed the interaction between recombinant 14-3-3 protein and synthetic fluorescein isothiocyanate (FITC)–labeled peptides containing phospho-Ser^{151} and a previously validated 14-3-3 binding motif of ARHGEF2 at phospho-Ser^{885} (*29*). Using microscale thermophoresis (MST), we demonstrated that 14-3-3 bound the phospho-Ser^{151} peptide [dissociation constant (K_d), 11.6 ± 1.9 μM] and the

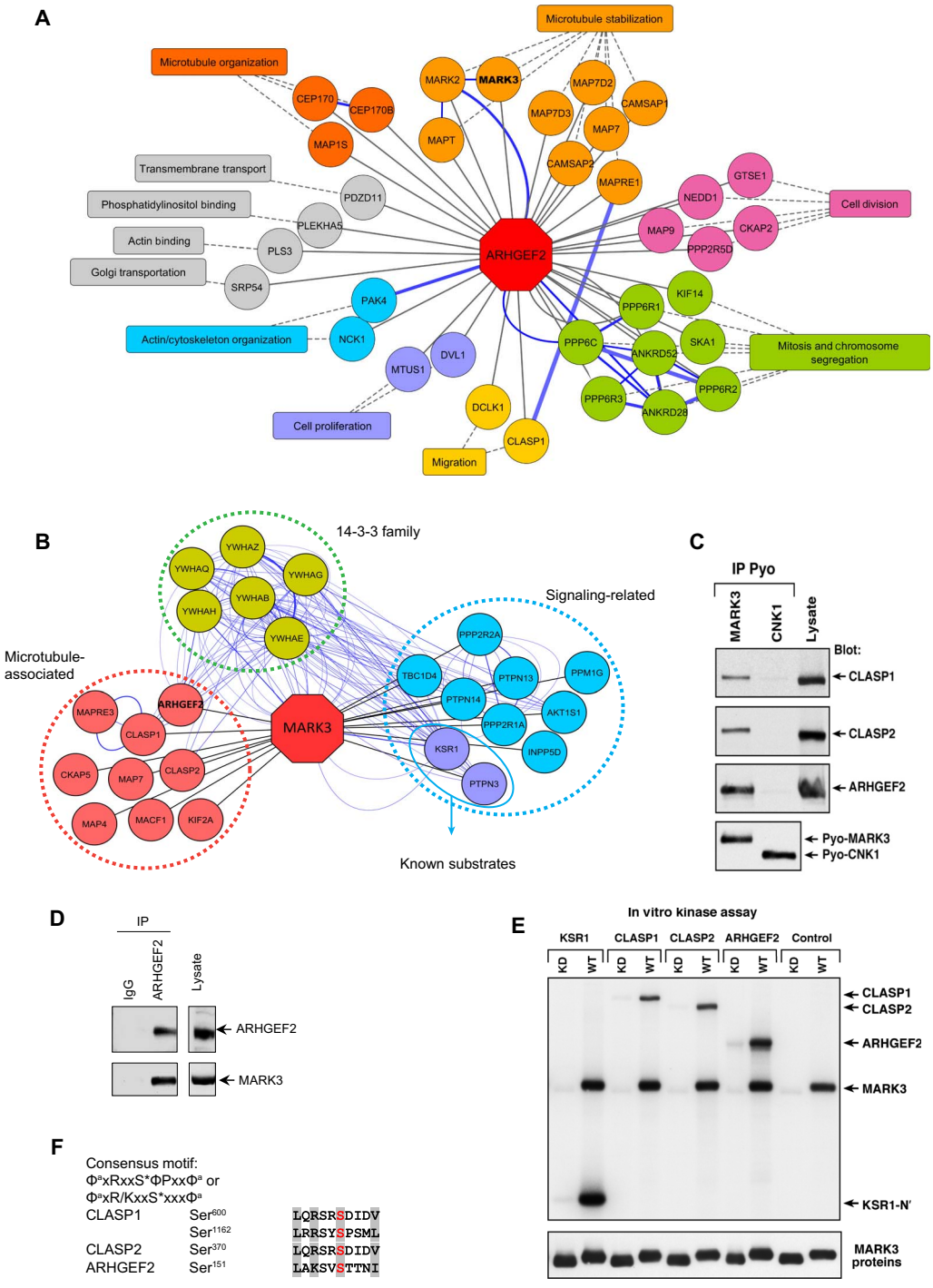

Fig. 1. Interaction networks of ARHGEF2 and MARK3. (**A**) ARHGEF2 high-confidence interactors detected by BioID MS (see table S1). Proteins with roles in similar biological processes are grouped by the indicated functions (see table S3), and reported protein-protein interactions (GeneMANIA) are highlighted with blue edges. (**B**) MARK3 interactors detected by MS of immunoprecipitated Pyo-MARK3 complexes (see table S4). Reported protein-protein interactions (GeneMANIA) are highlighted with blue edges. (**C**) Pyo-tagged wild-type MARK3 and CNK1 (negative control) were coexpressed with CLASP1, CLASP2, and ARHGEF2 and immunoprecipitated (IP) from Cos cell lysates. The protein complexes were examined by Western blotting using specific antibodies for CLASP1, CLASP2, and ARHGEF2 and Pyo for MARK3. (**D**) Cell lysates from human embryonic kidney (HEK) 293T cells were immunoprecipitated using immunoglobulin G (IgG) or an antibody recognizing ARHGEF2 combined with Sepharose beads. The protein complexes were separated by SDS–polyacrylamide gel electrophoresis (PAGE) and probed with antibodies recognizing MARK3 or ARHGEF2. Whole-cell lysates were analyzed by Western blotting to assess MARK3 and ARHGEF2 protein abundance. (**E**) KSR1 N′ (N-terminal head domain of KSR1), CLASP1, CLASP2, and ARHGEF2 proteins were immunoprecipitated from Cos cells and incubated with purified active wild-type (WT) or kinase-dead (KD) MARK3 in the presence of [γ-^{32}P]ATP. The labeled proteins were visualized by autoradiography and also Western-blotted to detect the purified MARK3 proteins. (C to E) Data are representative of three independent experiments. (**F**) Analysis of the protein sequences of CLASP1, CLASP2, and ARHGEF2 for the consensus MARK3 phosphorylation motifs Φ^axRxxS*ΦPxxΦ^a and Φ^axR/KxxS*xxxΦ^a using ScanProsite (S* is the site phosphorylated, x is any amino acid, Φ^a is a hydrophobic residue with an aliphatic side chain, and Φ is any hydrophobic amino acid).

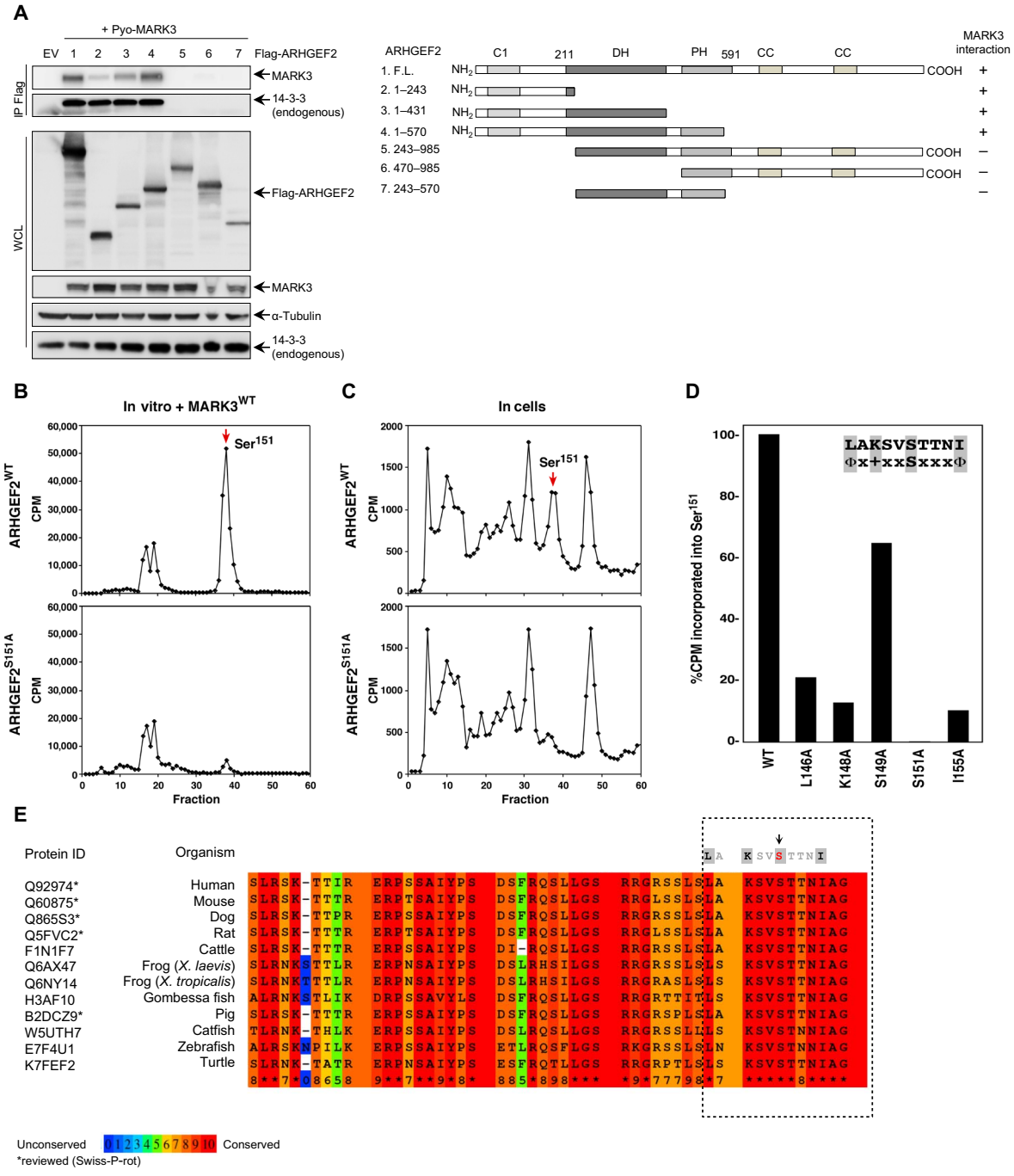

Fig. 2. MARK3 binds an N-terminal region of ARHGEF2 and phosphorylates Ser^{151}. (**A**) Left: Flag-tagged ARHGEF2 fragments and wild-type MARK3 were coexpressed in HEK293T cells. Protein complexes were immunoprecipitated, and immunoblots were probed with antibodies specific for MARK3 and pan 14-3-3 to map the interaction. Antibodies recognizing Flag, MARK, and 14-3-3 antibodies were used to detect protein abundance in cell lysates, and α-tubulin was used as a loading control. Right: Schematic representation of the constructs used for mapping the interaction. EV, empty vector; WCL, whole-cell lysates; F.L., full length. (**B** and **C**) ARHGEF2 wild-type (top) or mutant ARHGEF2^{S151A} (bottom) proteins were incubated with [^{32}P]ATP, digested with trypsin, and examined by high-performance liquid chromatography (HPLC) analysis. For the in vitro analysis (B), purified MARK3 was added. CPM, counts per minute. (**D**) Purified ARHGEF2 mutants were incubated with purified active MARK3 in the presence of [^{32}P]ATP. For each mutant, the [^{32}P]phosphate incorporated was quantitated using a phosphoimager. (A to D) Data are representative of three independent experiments. (**E**) Alignment of ARHGEF2 orthologs in vertebrates. The asterisks represent sequences reviewed by Swiss-Prot. The boxed area shows the consensus motif, and the color code is based on the conserved residues, with red being the most conserved. The full alignment is shown in fig. S2.

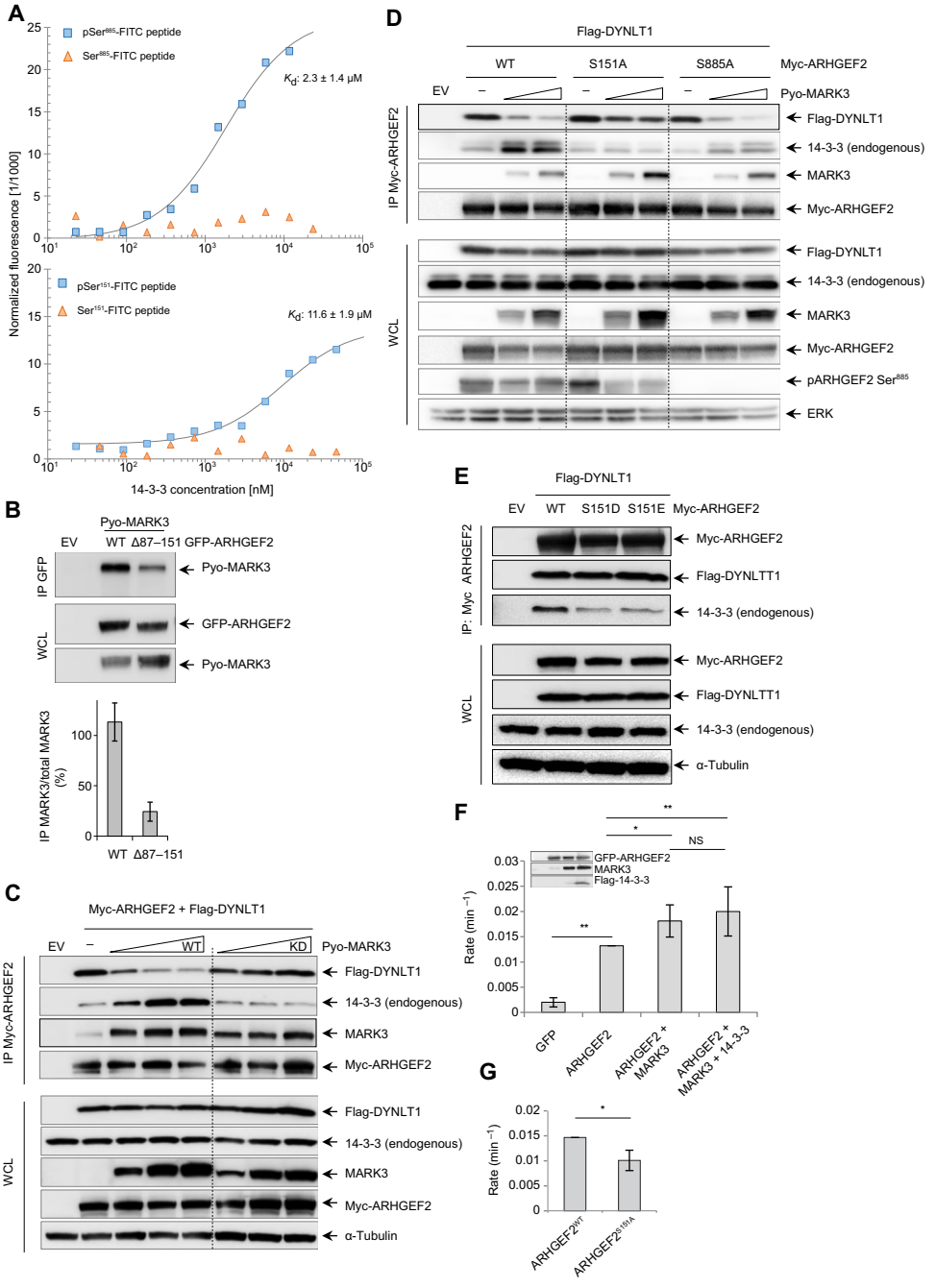

Fig. 3. MARK3 perturbs the interaction between DYNLT1 and ARHGEF2 and stimulates exchange activity. (**A**) MST binding assays of phosphorylated and unphosphorylated FITC-labeled ARHGEF2 peptides for Ser^{885} (amino acids 876 to 891; top) and Ser^{151} (amino acids 142 to 157; bottom). The peptides were prepared at 100 nM with increasing concentrations of glutathione *S*-transferase (GST)–14-3-3. K_d values were determined from the thermophoresis titration curves for the phosphorylated peptides, whereas no binding was detected for unphosphorylated peptides. K_d values are the average of three independent experiments ± SD. (**B**) Green fluorescent protein (GFP)–tagged wild-type ARHGEF2 and a truncated version (deletion of residues 87 to 151) were coexpressed with Pyo-tagged wild-type MARK3 in HEK293T cells. Protein complexes were immunoprecipitated using an antibody specific for GFP, and immunoblots were probed with antibodies recognizing Pyo to detect interactions with MARK3. Antibodies specific for GFP and Pyo were used to detect protein abundance in whole-cell lysates. Bottom: Quantification of the interaction normalized with total lysate. Data are means ± SD of three independent experiments. (**C**) Myc-tagged ARHGEF2 was coexpressed with Flag-tagged DYNLT1 in the absence or presence of increasing amounts of wild-type or kinase-deficient MARK3. Protein complexes were immunoprecipitated using an antibody recognizing Myc antibody and analyzed by Western blotting for the presence of MARK3, DYNLT1, and endogenous 14-3-3 using antibodies against MARK3, Flag, and pan 14-3-3, respectively. Whole-cell lysates were analyzed by Western blotting and probed with the same antibodies to assess protein abundance, and α-tubulin was used as a loading control (see also fig. S3, A and B, for quantification). Data are representative of four independent experiments. (**D**) Myc-tagged wild-type ARHGEF2 and S151A and S885A mutants were coexpressed with Flag-tagged DYNLT1 in the absence or presence of increasing amounts of wild-type MARK3 in HEK293T cells. Protein complexes were immunoprecipitated using an antibody recognizing Myc and analyzed by Western blotting for the presence of MARK3, DYNLT1, and endogenous 14-3-3 using antibodies against MARK3, Flag, and 14-3-3, respectively. Whole-cell lysates were analyzed with the same antibodies to assess protein abundance. Total extracellular signal–regulated kinase (ERK) was used as a loading control (see fig. S3C for quantification). Data are representative of three independent experiments. (**E**) Myc-tagged wild-type and phosphomimetic mutants S151D and S151E for ARHGEF2 were coexpressed with Flag-tagged DYNLT1. Protein complexes were immunoprecipitated with an antibody recognizing Myc and analyzed by Western blotting. Antibodies against Myc, Flag, and 14-3-3 were used to confirm the amount of ARHGEF2 and to detect DYNLT1 and endogenous 14-3-3 in the complexes, respectively. Protein abundance in whole-cell lysates was analyzed using the same antibodies, and α-tubulin was used as a loading control. Data are representative of three independent experiments. (**F**) NMR-based GEF assays were performed to measure RHOA exchange rates in the presence of cell lysates from HEK293T cells expressing GFP alone; GFP-ARHGEF2; GFP-ARHGEF2 and Pyo-MARK3; or GFP-ARHGEF2, Pyo-MARK3, and Flag-14-3-3. The amount of ARHGEF2 in exchange assays was normalized on the basis of GFP fluorescence in the lysate, and protein amounts were detected by Western blotting (inset). The rates were normalized to ARHGEF2 exchange rate. Data are means ± SD of five independent experiments. Statistical significance was determined by a Kruskal-Wallis test with a Dunn's posttest correction for multiple comparisons. *P = 0.0151 (ARHGEF2 compared to ARHGEF2 + MARK3); **P = 0.0072 (ARHGEF2 compared to ARHGEF2 + MARK3 + 14-3-3); **P = 0.0079 (GFP compared to ARHGEF2). NS, not significant. (**G**) Nucleotide exchange rates for RHOA in the presence of cell lysates from HEK293T cells expressing GFP-ARHGEF2^{WT} or GFP-tagged ARHGEF2^{S151A}. The rates were normalized to ARHGEF2^{WT} exchange rate. Data are means ± SD of four independent experiments. Statistical significance was determined by a Mann-Whitney test. *P = 0.0286.

phospho-Ser^{885} ARHGEF2 peptide (K_d, 2.3 ± 1.4 μM), both in a phosphorylation-dependent manner (Fig. 3A).

MARK3 regulates a phosphorylation-dependent switch that controls the localization and activity of ARHGEF2

We have previously mapped the DYNLT1-binding site on ARHGEF2 to residues 139 to 161 (*27*). The MARK3 phosphorylation site is located within this DYNLT1-binding site, suggesting that phosphorylation or the subsequent binding of 14-3-3 proteins could potentially disrupt the interaction between DYNLT1 and ARHGEF2. An ARHGEF2 mutant lacking amino acids 87 to 151 no longer binds to DYNLT1 or microtubules and is highly active (*27*). Deletion of these residues also diminished the interaction of MARK3 with ARHGEF2, suggesting that the MARK3 binding site overlaps with residues 87 to 151 (Fig. 3B). Because MARK3 and DYNLT1 bind to a similar region of ARHGEF2, we investigated whether MARK3 affected the interaction between ARHGEF2 and DYNLT1. We observed that increased amounts of MARK3 potently decreased the association of ARHGEF2 with DYNLT1 (Fig. 3C and fig. S3A).

We also noted that the amount of 14-3-3 in complex with ARHGEF2 tended to increase with MARK3 expression (Fig. 3C and fig. S3B) but that MARK3^{KD} did not directly compete with DYNLT1. These results demonstrated that MARK3 kinase activity was required both to increase the interaction with 14-3-3 and to disrupt the DYNLT1-ARHGEF2 interaction (Fig. 3C). To probe the requirement of Ser^{151} to mediate the MARK3-dependent displacement of DYNLT1, we compared the interaction of DYNLT1 with ARHGEF2^{WT} or ARHGEF2^{S151A} in the presence of increasing amounts of MARK3. Increasing MARK3 expression increased 14-3-3 and reduced DYNLT1 bound to wild-type ARHGEF2 but not to the S151A mutant (Fig. 3, C and D, and fig. S3C). By contrast, the S885A mutant exhibited less overall interaction with 14-3-3 proteins, consistent with disruption of this known binding site; however, binding of 14-3-3 was increased, whereas DYNLT1 binding was decreased, by MARK3 in the same manner as wild type (Fig. 3D and fig. S3C). These data suggested that Ser^{151} was phosphorylated by MARK3 to create a 14-3-3 binding site that excluded binding to DYNLT1. In contrast, the C-terminal 14-3-3 binding site centered around Ser^{885} had no effect on DYNLT1 interaction with ARHGEF2.

To investigate whether the addition of a negative charge on Ser^{151} as a result of phosphorylation was sufficient to disrupt the interaction of DYNLT1 with ARHGEF2, we generated two distinct Ser^{151} phosphomimetic ARHGEF2 mutants by substituting the negatively charged amino acids aspartic acid (D) or glutamic acid (E) at position 151 and observed no effect on DYNLT1 binding. Both of these mutants exhibited reduced 14-3-3 binding, consistent with the inability of 14-3-3 to bind to phosphomimetic residues (Fig. 3E) (*44*, *45*). These results indicate that MARK3 phosphorylation promoted binding of 14-3-3 within the DYNLT1 interaction sequence of ARHGEF2 to disrupt the interaction between the dynein and the guanine exchange factor, potentially affecting the microtubule-tethered inhibited state of ARHGEF2.

To determine how MARK3 might regulate the exchange factor activity of ARHGEF2, we used a real-time nuclear magnetic resonance (NMR)–based assay (*27*, *46*) to measure the exchange activity. MARK3 coexpression with ARHGEF2 increased the rate of RHOA nucleotide exchange, and expression of MARK3 together with 14-3-3 further increased the exchange activity of ARHGEF2 (Fig. 3F and inset). Mutation of the MARK3 Ser^{151} phosphorylation site on ARHGEF2 decreased its GEF activity (Fig. 3G). These data support a model that MARK3 regulates a phospho-switch that leads to both the displacement of ARHGEF2 from microtubules and its concomitant activation.

Ser^{151} in ARHGEF2 is localized in the core of the DYNLT1-binding groove

To investigate whether the phosphorylation of ARHGEF2 on Ser^{151} directly controls the interaction between ARHGEF2 and DYNLT1, we measured the binding affinities between a nonphosphorylated FITC-labeled 16-mer peptide derived from ARHGEF2 (residues 142 to 157) or a peptide phosphorylated on Ser^{151} to recombinant GST-tagged DYNLT1. Fluorescence polarization assays showed that phosphorylation had no direct impact on binding (Fig. 4A; see also Fig. 3E). The murine ARHGEF2 peptide (residues 133 to 161) interacts with DYNLT1 with low affinity (K_d, 80 μM) (*27*), resulting in line broadening of the resonances of both the peptide and the protein. This hindered our efforts to determine a high-resolution structure of the DYNLT1-ARHGEF2 complex by NMR and to crystallize the complex.

To capture the bound state of the ARHGEF2 peptide to DYNLT1 for crystallographic and NMR structural studies, we coupled the ARHGEF2 (residues 136 to 164) peptide to DYNLT1 using a flexible linker to enhance the apparent affinity of the interaction (*47*). The binding orientation of the ARHGEF2 peptide was determined using paramagnetic relaxation enhancement experiments using a synthetic ARHGEF2 peptide (ARHGEF2-Cys^{137}-Trp^{158}) with an N-terminal cysteine conjugated to a maleimide-linked EDTA tag to chelate a paramagnetic ion (fig. S4A). DYNLT1 residues proximal to the N terminus of the peptide were identified by broadening of their ^{15}N-^{1}H heteronuclear single-quantum correlation (HSQC) cross peaks in the presence of Mn^{2+}-bound peptide compared to Ca^{2+}-bound peptide. Mapping the perturbed peaks onto the DYNLT1 structure revealed a patch near the C terminus of DYNLT1 comprising Ser^{88} and Ile^{113} (fig. S4B). Thus, we fused the ARHGEF2 peptide to the C terminus of DYNLT1, initially connected by a long flexible linker (GLEGGSGGSG), to facilitate native interaction.

A comparison of the ^{15}N-^{1}H HSQC spectra of the ^{15}N-labeled chimera with that of ^{15}N-labeled DYNLT1 in the presence of excess unlabeled ARHGEF2 (residues 136 to 161) peptide validated that within the chimera ARHGEF2 bound DYNLT1 in the native manner and saturated the site more fully (Fig. 4B). Using these spectra to assess native interaction, the linker was progressively shortened (from GLEGGSGGSG to GGSGGSG to G) to remove unnecessary flexible regions. A single glycine linker was sufficient to maintain the native "fingerprint" spectrum, reduce peak broadening, and increase saturation of the binding site. Fifty-two percent of the backbone resonances of this chimera were assigned. Whereas the apo form of murine DYNLT1 did not produce crystals despite extensive screening (~600 unique crystallization conditions), the chimera was readily crystallized in numerous conditions that were further optimized to generate a crystal that diffracted to high resolution.

The crystal structure of the chimera had three molecules per asymmetric unit, two of which formed a homodimer, whereas the third formed a dimer with a symmetrically related molecule (fig. S4C and table S5). Similar to previously determined DYNLT1 homolog structures, each subunit had two α helices that flanked a central β sheet consisting of four strands (β2′, β1, β4, and β3), one of which (β2) was domain-swapped from the other subunit (Fig. 4C). Because of the absence of electron density, residues 1 to 4 and 73 to 76 of DYNLT1 and residues 136 to 138 and 156 to 164 of ARHGEF2 were not built into the model. ARHGEF2 residues 140 to 155 lay in the grooves formed at the interface of the two homodimeric DYNLT1 subunits. Residues 140 to 144 formed one turn of 3_{10} helix, whereas residues 145 to 147 and 153 to 155 had β-strand characteristics with nine backbone hydrogen bonds

formed between this stretch of the ARHGEF2 peptide (residues 145 to 155) and DYNLT1 (Fig. 4D). An H-bond between ARHGEF2 Ala^{147} and DYNLT1 Cys^{83} was consistent with nuclear Overhauser effects (NOEs) observed between these residues in solution (fig. S4D). ARHGEF2 bound to the edge of the β sandwich, extending the domain-swapped antiparallel β sheet of DYNLT1 (Fig. 4C). Relative to a perfect β strand, ARHGEF2 contained two extra amino acids, which were accommodated in the binding site through a distortion of the β strand (an antiparallel β bulge comprising two type IV β turns) (Fig. 4D). The β bulge disrupted the classic antiparallel β-sheet hydrogen bonding network

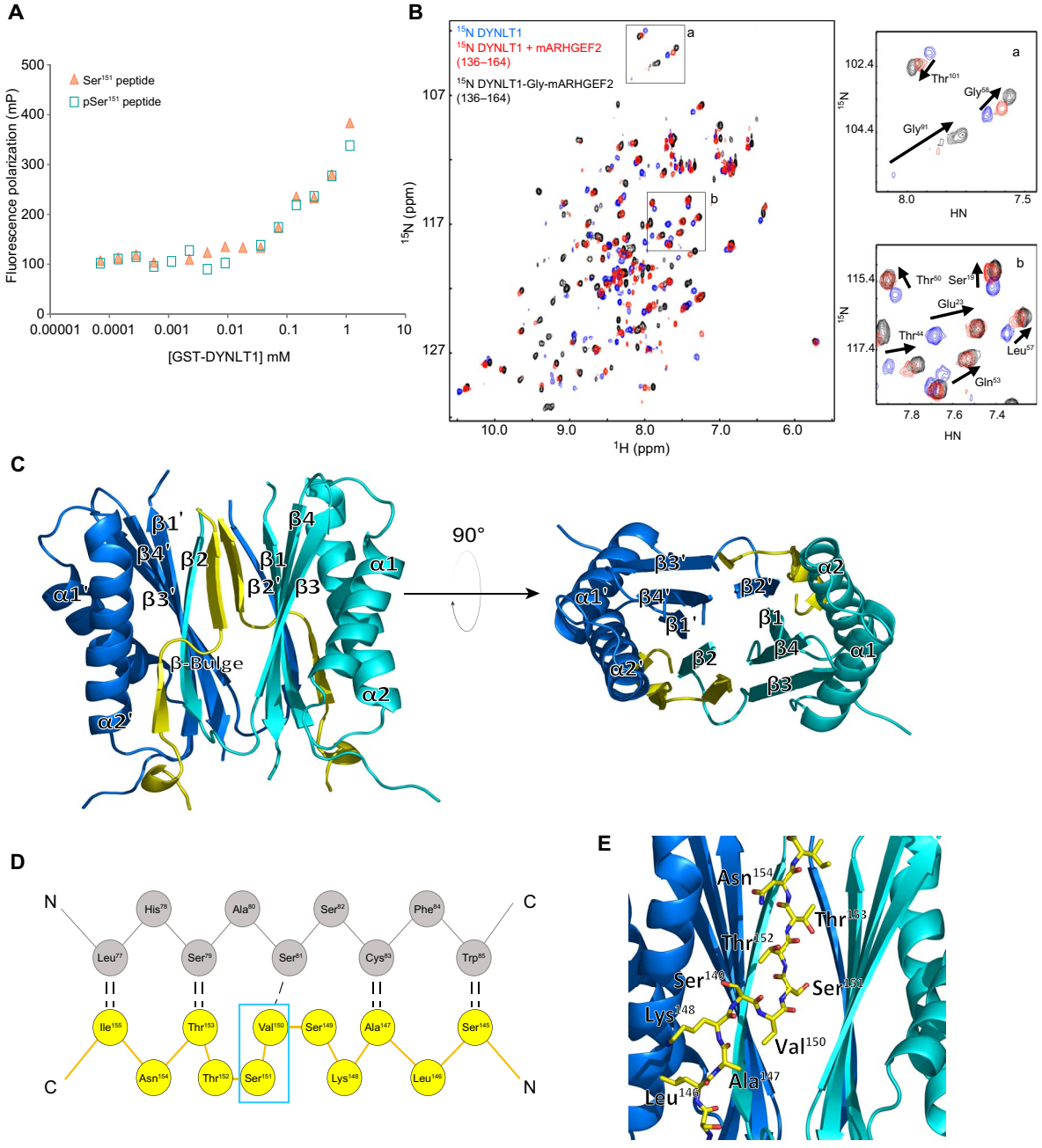

Fig. 4. Structural characterization of the DYNLT1-ARHGEF2 interaction. (**A**) Fluorescence polarization binding assays were performed with FITC-labeled ARHGEF2 peptides (residues 142 to 157) with and without the phosphorylation of Ser^{151}. The peptides were titrated with increasing amounts of recombinant GST-DYNLT1. Data are representative of two independent experiments. mP, millipolarization units. (**B**) Overlay of ^{1}H-^{15}N HSQC spectra of DYNLT1 in the absence (blue) or presence (red) of mARHGEF2 peptide (residues 136 to 164) or in the context of a DYNLT1:mARHGEF2 chimera with a single glycine linker (black). Inset boxes (a and b) zoom into the overlay of the spectra. Chemical shift changes for selected residues are highlighted with arrows in the spectra. ppm, parts per million. (**C**) Structure of DYNLT1:ARHGEF2 chimera [Protein Data Bank (PDB): 5WI4] (see fig. S4C for the asymmetric unit and crystallographic contact sites). Ribbon representation: Blue and cyan are used to distinguish the two subunits of DYNLT1. The ARHGEF2 portion is yellow. (**D**) Schematic representation of interactions between the domain-swapped β strand of DYNLT1 and ARHGEF2. Residues of DYNLT1 (gray) and ARHGEF2 (yellow) with the hydrogen bond network are shown by black dashed lines. A kink in ARHGEF2 is caused by the insertion (relative to a perfect β strand) of residues Val^{150} and Ser^{151} (cyan box), which form a β bulge. (**E**) Detail of DYNLT1 in complex with ARHGEF2. Enlargement showing the ribbon representation of DYNLT1 (blue) with a stick model of the mARHGEF2 (yellow) component of the chimera (PDB: 5WI4). ARHGEF2 residues Leu^{146} to Asn^{154} are highlighted.

(*48*, *49*): Ser^{151} did not participate in backbone hydrogen bonding with DYNLT1 in two crystallographically independent subunits, and residues Ser^{149}, Val^{150}, and Ser^{151} exhibited large deviations from the ideal β-sheet φ/ψ dihedral angles. The structure revealed that ARHGEF2 Ser^{151} was in the core of the DYNLT1-binding site (Fig. 4E), providing a clear structural basis for the observed competition between DYNLT1 and 14-3-3 for interaction with ARHGEF2. The side-chain hydroxyl of Ser^{151} was closely packed and formed hydrogen bonds with the hydroxyls of DYNLT1 Thr^{94} and Ser^{107} (fig. S4E); thus, Ser^{151} phosphorylation would introduce a steric clash in this conformation. However, because our in vitro and in vivo observations indicated that phosphorylation alone or phosphomimetic mutations do not disrupt this complex, we propose that flexibility of the β bulge may allow these residues to adopt an alternate conformation in which a phosphorylated Ser^{151} side chain can be accommodated in the binding groove. Several structural observations suggested that the β bulge exhibits some conformational dynamics. Besides the hydrogen bonds mediated by the Ser^{151} hydroxyl, which would be disrupted upon phosphorylation, and a few bound water molecules, there were few interactions stabilizing the β bulge. Thus, its conformation diverged slightly among each of the three molecules in the asymmetric unit. In NMR experiments, a stretch of four ARHGEF2 amino acids (Leu^{144} to Ala^{147}) in the chimera were assigned; however, broadening of resonances from the β-bulge residues was consistent with the presence of multiple interconverting conformations. Further, phosphorylation of DYNLT1 Thr^{94} or phosphomimetic mutation (T94E) disrupts its interaction with dynein intermediate chain (DIC) (*50*), which lacks the β bulge at this site (*51*), but $DYNLT1^{T94E}$ retains binding to ARHGEF2 (*27*). The DYNLT1-binding region of ARHGEF2 is remarkably rich in phosphorylation sites (Ser^{143}, Ser^{149}, Ser^{151}, Thr^{152}, Thr^{153}, and Ser^{163}) that have been reported in previous proteomics studies (*33*, *35*, *52*–*56*) and could potentially modulate this interaction. The modest affinity of DYNLT1 for monomeric ARHGEF2 peptide would allow kinases to gain access to their phosphorylation motifs, whereas the tethering of ARHGEF2 to microtubules is likely enhanced by avidity in multivalent protein complexes (*57*). A structure of mammalian DYNLT1 in complex with the DIC polypeptide (*58*) has also been determined using this chimeric approach (*59*).

PP2A and MARK3 regulate the phosphorylation of Ser^{151} in ARHGEF2

The PP2A phosphatase promotes mitogen-activated protein kinase (MAPK) signaling by mediating the dephosphorylation of critical 14-3-3 binding sites in KSR1 that are phosphorylated by MARK3 (*60*) and is also the major phosphatase for different MAPs (*61*, *62*). Treatment of cells with a low dose of okadaic acid (OA), an inhibitor of PP2A family phosphatases, resulted in an increase in ARHGEF2 Ser^{151} phosphorylation as assessed by phospho-Ser^{151}–specific antibodies (fig. S5A), suggesting that PP2A or a related phosphatase dephosphorylated this residue (Fig. 5A). Because ARHGEF2 Ser^{151} has been identified in a high-throughput screen as a substrate of AMPK (*56*), we also treated the cells with the AMPK activator 5-aminoimidazole-4-carboxamide ribonucleotide (AICAR), but no apparent change in the phosphorylation of this residue was observed (Fig. 5A).

To verify whether PP2A modulated regulatory phosphosites on ARHGEF2, we overexpressed the serine-threonine PP2A 56-kDa regulatory subunit β isoform (PPP2R5B), a member of the B′ regulatory subunit of PP2A that specifically interacts with and modulates ARHGEF2 (*26*, *30*), in HEK293T cells and observed that both Ser^{151} and Ser^{885} were efficiently dephosphorylated (Fig. 5B). We also used tetracycline-inducible (TETi) cell lines expressing Flag-tagged catalytic PPP2CB and regulatory PPP2R5B subunits of PP2A in the presence of $MARK3^{WT}$ or $MARK3^{KD}$ and observed that these PP2A subunits each tended to decrease the phosphorylation of Ser^{151}, whereas coexpression of $MARK3^{WT}$ but not $MARK3^{KD}$ increased Ser^{151} phosphorylation (Fig. 5C). No evident changes in Ser^{151} phosphorylation were observed when another ARHGEF2-associated phosphatase, PPP6C (Fig. 1A), was overexpressed, suggesting that PP2A specifically dephosphorylates ARHGEF2 Ser^{151} (fig. S5B).

LKB1 promotes the phosphorylation of ARHGEF2 Ser^{151} through MARK3

Members of the family of MARKs are downstream targets of the serine-threonine kinase liver kinase B1 (LKB1; also known as STK11 and Par-4) (*63*–*65*). LKB1 is a tumor suppressor linked to Peutz-Jeghers syndrome (*66*, *67*) and plays a key role in establishing cell polarity in *Drosophila*, *C. elegans*, and mammals (*68*–*70*). We probed Ser^{151} phosphorylation in the *LKB1*-deficient non–small cell lung cancer cell line A549 stably expressing wild-type LKB1 ($LKB1^{WT}$), kinase-dead LKB1 ($LKB1^{KD}$), or empty vector (pBabe), as previously described (*71*). ARHGEF2 phospho-Ser^{151} was detectable at low abundance in the control cells but was strongly enhanced in $LKB1^{WT}$ cells. Expression of $LKB1^{KD}$ had little impact on the amount of phospho-Ser^{151} (Fig. 5D). To interrogate the role of MARK3 as the potential downstream kinase regulated by LKB1 responsible for the phosphorylation of ARHGEF2 on Ser^{151}, we knocked down *MARK3* in $LKB1^{WT}$ cells and observed decreased Ser^{151} phosphorylation but not AMPK phosphorylation. These data provide genetic evidence that LKB1 enhanced Ser^{151} phosphorylation through activation of MARK3 (Fig. 5E).

MARK3-mediated phosphorylation of ARHGEF2 triggers its redistribution from microtubules to the cytoplasm

Binding of 14-3-3 proteins to the MARK3 phosphorylated substrates KSR-1, CDC25C, and PKP2 is associated with alteration in their subcellular localization (*40*, *72*, *73*). We tested whether the phosphorylation of Ser^{151} altered the localization of ARHGEF2. Confocal microscopy of transfected HEK293T cells revealed that GFP-tagged wild-type ARHGEF2 ($GFP\text{-}ARHGEF2^{WT}$) was localized to microtubule-like filamentous structures, as previously described (Fig. 6, A and B) (*27*, *28*). MARK3 coexpression disrupted the filament-like localization of $GFP\text{-}ARHGEF2^{WT}$, inducing a diffuse and uniform cytoplasmic distribution. In contrast, $GFP\text{-}ARHGEF2^{S151A}$ was strongly associated with microtubule-like filamentous structures with some bundling, which was resistant to coexpression of MARK3 (Fig. 6, A and B).

To determine the requirement of MARK3 in determining the subcellular localization of ARHGEF2, we overexpressed $ARHGEF2^{WT}$ or $ARHGEF2^{S151A}$ at low amounts under the control of a TETi promoter in MDCKII cells (pLVX-GFP $ARHGEF2^{WT}$ or pLVX-GFP $ARHGEF2^{S151A}$, respectively) (fig. S6, A and B). We observed a diffused distribution of $GFP\text{-}ARHGEF2^{WT}$ (Fig. 6C). After knockdown of *MARK3* using siRNA (fig. S6C), we observed that a larger fraction of $GFP\text{-}ARHGEF2^{WT}$ was associated with microtubule-like filamentous structures in the absence of MARK3 and tended to phenocopy the subcellular filament-like distribution of $GFP\text{-}ARHGEF2^{S151A}$ (Fig. 6, C and D). These data demonstrate that MARK3-dependent phosphorylation of ARHGEF2 promoted its dissociation from the filamentous structures in the cell.

Phosphorylation of ARHGEF2 on Ser^{151} by MARK3 promotes stress fibers and focal adhesion formation

ARHGEF2 overexpression promotes RHOA activation and induces the formation of stress fibers and focal adhesions (*27*). We examined the

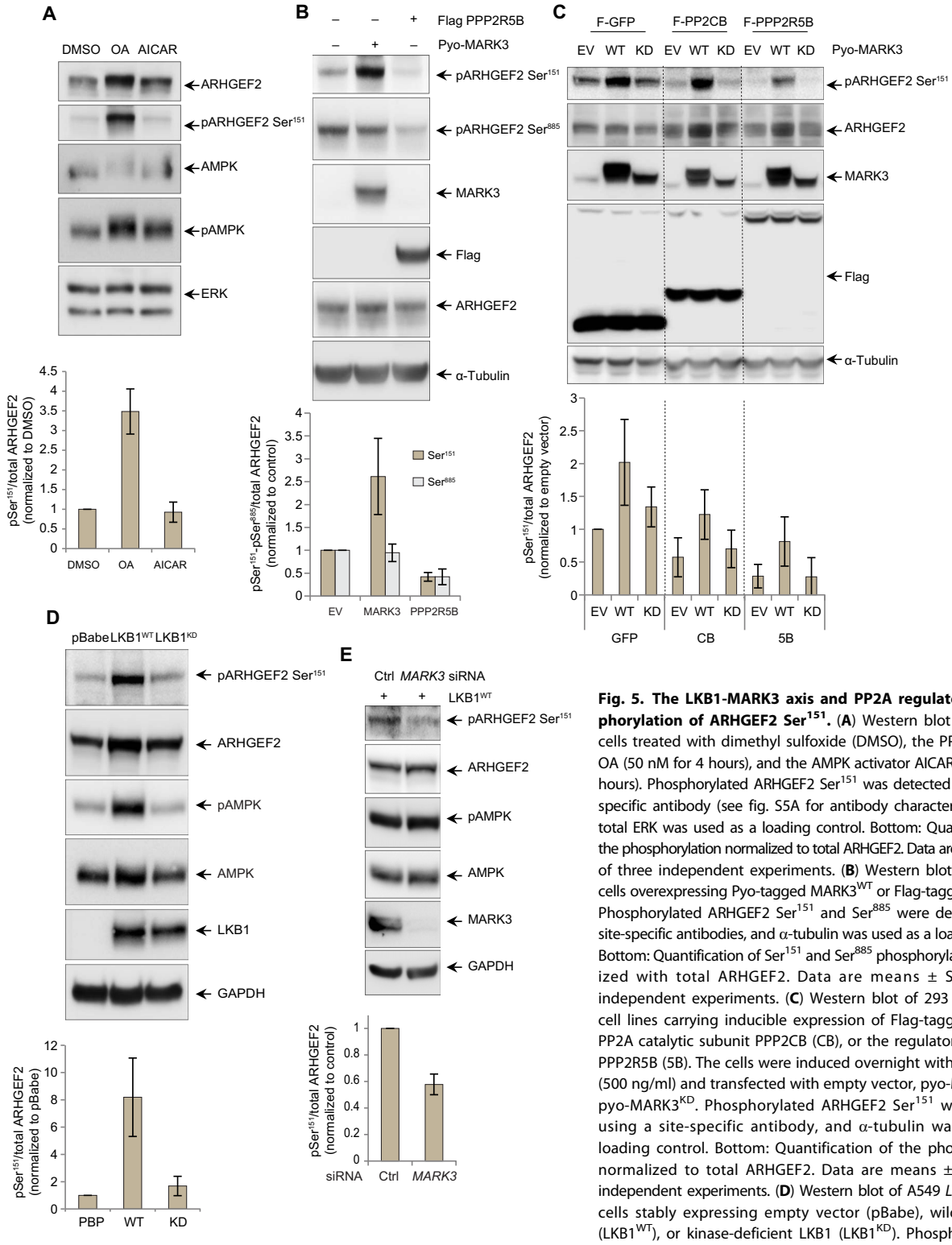

Fig. 5. The LKB1-MARK3 axis and PP2A regulate the phosphorylation of ARHGEF2 Ser^{151}. (**A**) Western blot of HEK293T cells treated with dimethyl sulfoxide (DMSO), the PP2A inhibitor OA (50 nM for 4 hours), and the AMPK activator AICAR (1 mM for 6 hours). Phosphorylated ARHGEF2 Ser^{151} was detected using a site-specific antibody (see fig. S5A for antibody characterization), and total ERK was used as a loading control. Bottom: Quantification of the phosphorylation normalized to total ARHGEF2. Data are means ± SD of three independent experiments. (**B**) Western blot of HEK293T cells overexpressing Pyo-tagged MARK3^{WT} or Flag-tagged PPP2R5B. Phosphorylated ARHGEF2 Ser^{151} and Ser^{885} were detected using site-specific antibodies, and α-tubulin was used as a loading control. Bottom: Quantification of Ser^{151} and Ser^{885} phosphorylation normalized with total ARHGEF2. Data are means ± SD of three independent experiments. (**C**) Western blot of 293 Flp-In T-REx cell lines carrying inducible expression of Flag-tagged GFP, the PP2A catalytic subunit PPP2CB (CB), or the regulatory B′ subunit PPP2R5B (5B). The cells were induced overnight with tetracycline (500 ng/ml) and transfected with empty vector, pyo-MARK3^{WT}, or pyo-MARK3^{KD}. Phosphorylated ARHGEF2 Ser^{151} was detected using a site-specific antibody, and α-tubulin was used as a loading control. Bottom: Quantification of the phosphorylation normalized to total ARHGEF2. Data are means ± SD of four independent experiments. (**D**) Western blot of A549 *LKB1*-deficient cells stably expressing empty vector (pBabe), wild-type LKB1 (LKB1^{WT}), or kinase-deficient LKB1 (LKB1^{KD}). Phosphorylation of AMPK was used as a control substrate for LKB1 phosphorylation. Phosphorylated ARHGEF2 Ser^{151} and AMPK Thr^{172} were detected using site-specific antibodies, and glyceraldehyde-3-phosphate dehydrogenase (GAPDH) was used as a loading control. Bottom: Quantification of ARHGEF2 Ser^{151} phosphorylation normalized with total ARHGEF2. PBP, pBabe-puromycin (empty vector). Data are means ± SD of three independent experiments. (**E**) Western blot of A549 cells expressing LKB1^{WT} and treated with a small interfering RNA (siRNA) pool specific for MARK3 or control siRNA for 72 hours. AMPK was used as a control substrate for LKB1-mediated phosphorylation. GAPDH was used as a loading control. Bottom: Quantification of ARHGEF2 Ser^{151} phosphorylation normalized with total ARHGEF2. Data are means ± SD of three independent experiments.

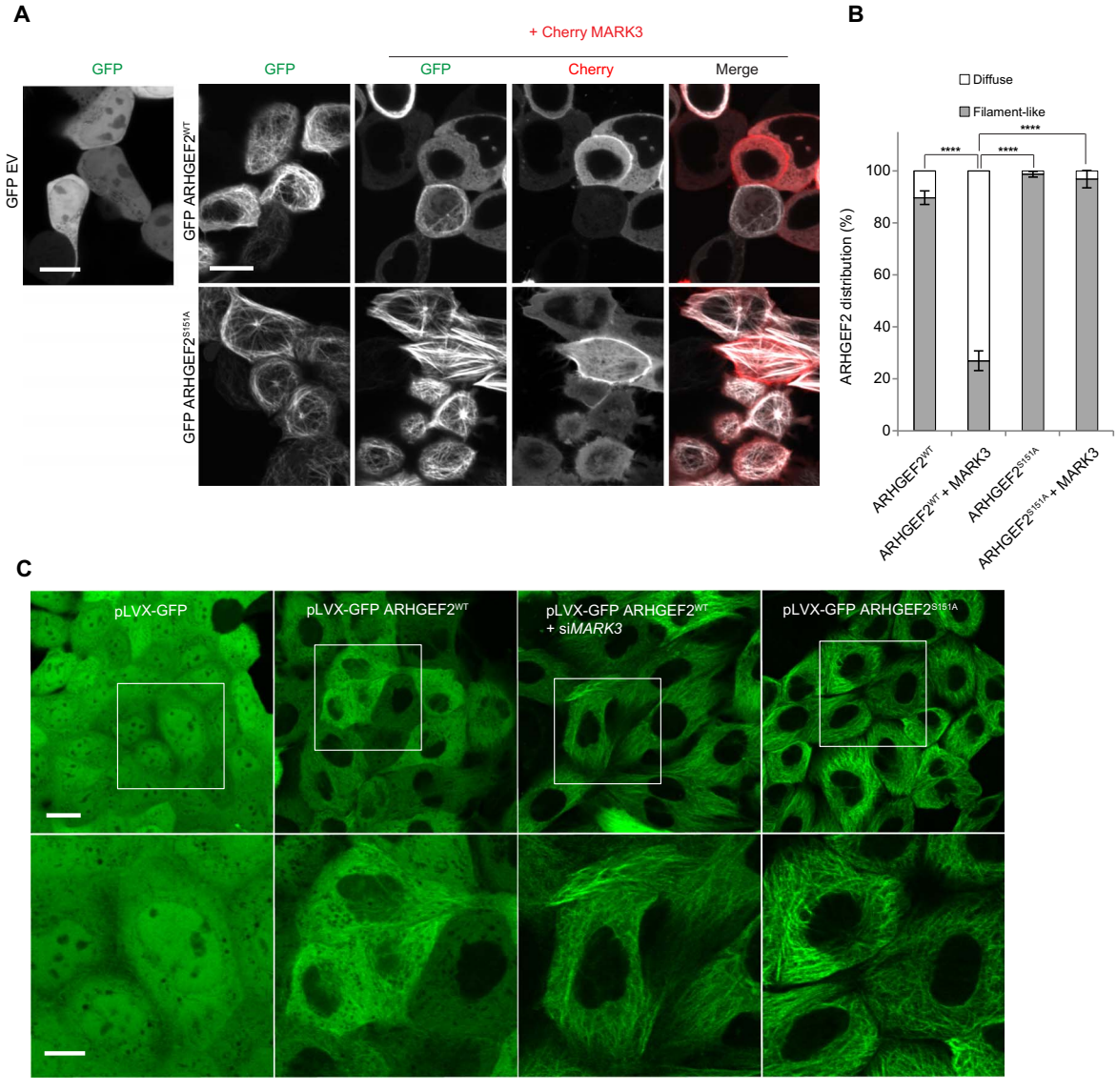

Fig. 6. MARK3 affects the localization of ARHGEF2 dependent on Ser^{151} and 14-3-3. (**A** and **B**) Live imaging of HEK293T cells. (A) Top: Cells transiently overexpressing GFP alone and GFP-ARHGEF2^{WT}, alone or in combination with Cherry-MARK3; bottom: cells expressing GFP-ARHGEF2^{S151A} alone or coexpressed with Cherry-MARK3. ARHGEF2 distribution in (A) is quantified in (B) (as percentage of cells). A total of 100 to 200 cells per condition were counted. Data are means ± SD of three independent experiments (n = 3). Scale bars, 10 μm. Statistical significance was determined by a two-way analysis of variance (ANOVA) test with a Bonferroni posttest correction for multiple comparisons. ****$P \leq 0.0001$. (**C** and **D**) Live imaging of MDCKII cells stably expressing inducible pLVX-GFP, pLVX-GFP ARHGEF2^{WT}, pLVX-GFP ARHGEF2^{S151A}, and pLVX-GFP ARHGEF2^{WT} in combination with si*MARK3*; zoomed regions are shown in bottom panels. Scale bars, 20 μm (top) and 10 μm (bottom). (D) Quantification, as percentage of cells, of images in (C): cells having a higher tendency of showing a filament-like distribution (F > D), a higher tendency of having a diffuse distribution (D > F), or similar distribution of filament-like and diffuse-appearing structures (D = F). F, filament-like distribution; D, diffuse distribution. A total of 250 to 300 cells per condition were counted. Data are means ± SD of three independent experiments. Statistical significance was determined by a two-way ANOVA test with a Bonferroni posttest correction for multiple comparisons. *P = 0.0470 (in F > D; ARHGEF2^{WT} compared to ARHGEF2^{WT} + si*MARK3*); *P = 0.0235 (in F = D; ARHGEF2^{WT} compared to ARHGEF2^{WT} + si*MARK3*); **P = 0.0014; ***P = 0.0002 (in F > D; ARHGEF2^{WT} + si*MARK3* versus ARHGEF2^{S151A}); ***P = 0.0005 (in D > F; ARHGEF2^{WT} compared to ARHGEF2^{WT} + si*MARK3*); ****$P \leq 0.0001$.

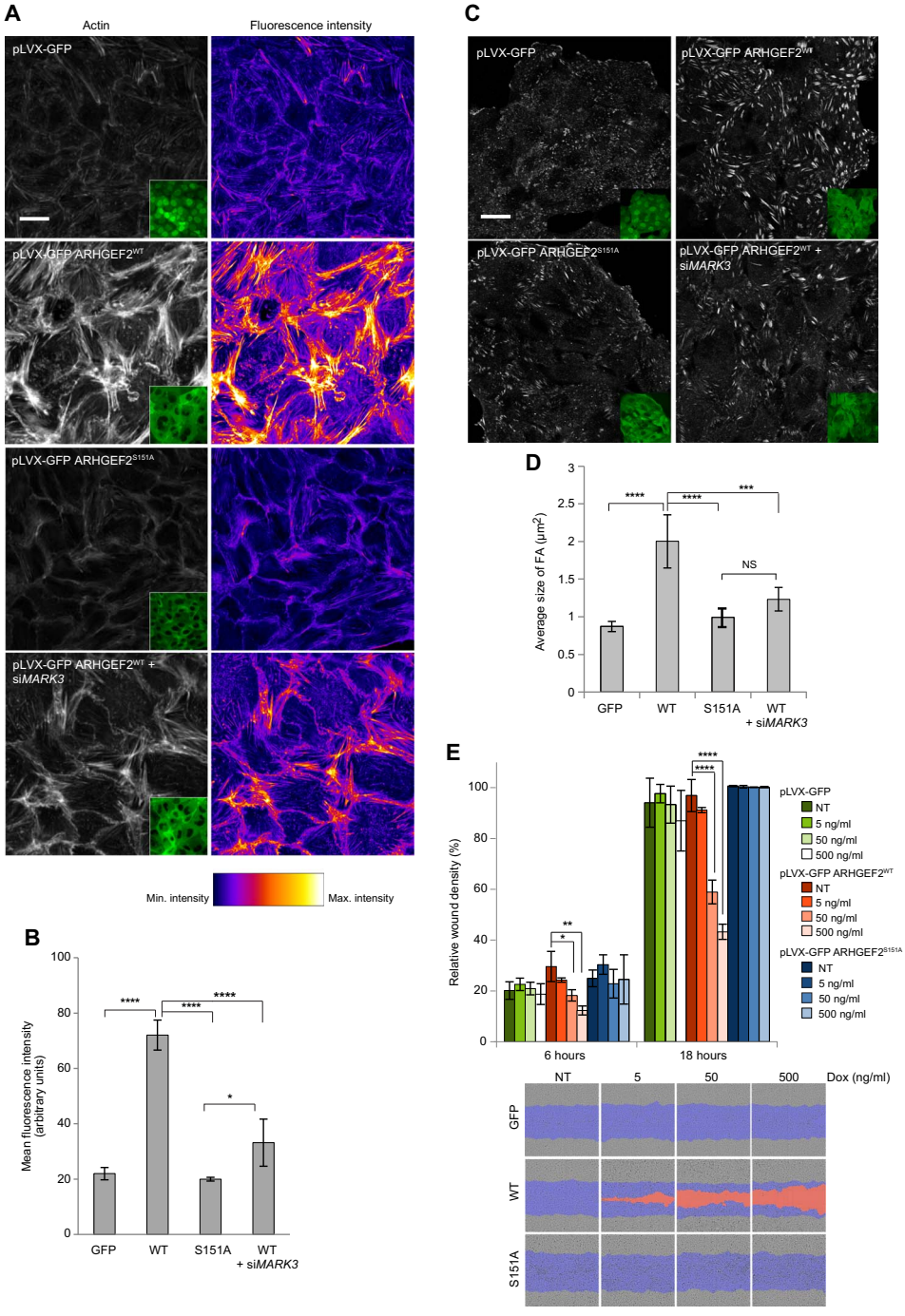

Fig. 7. MARK3 phosphorylation of ARHGEF2 Ser^{151} regulates several biological functions. (**A** and **B**) Immunofluorescence of MDCKII cells stably expressing inducible pLVX-GFP, pLVX-GFP ARHGEF2^{WT}, pLVX-GFP ARHGEF2^{S151A}, and pLVX-GFP ARHGEF2^{WT} with si*MARK3*. Left: The cells were fixed and stained for actin; GFP signal is shown (inset). Right: Lookup tables showing the fluorescence intensity, with white denoting maximum intensity. (B) Quantification of the mean fluorescence intensity of five high-magnification fields per condition and per experiment for the images in (A). Data are means ± SD of three independent experiments. Scale bar, 20 μm. Statistical significance was determined by a one-way ANOVA test with a Bonferroni posttest correction for multiple comparisons. *P = 0.0453; ****$P \leq$ 0.0001. (**C** and **D**) Immunofluorescence of MDCKII cells stably expressing inducible pLVX-GFP, pLVX-GFP ARHGEF2^{WT}, pLVX-GFP ARHGEF2^{S151A}, and pLVX-GFP ARHGEF2^{WT} with si*MARK3*. The cells were fixed and stained for vinculin; GFP signal is shown (inset). (D) Quantification of the average size of the focal adhesion (FA) from four high-magnification fields per condition and per experiment of the images shown in (C). Data are means ± SD of three independent experiments. Scale bar, 20 μm. Statistical significance was determined by a one-way ANOVA test with a Bonferroni posttest correction for multiple comparisons. ***P = 0.0010; ****$P \leq$ 0.0001. (**E**) Relative wound density (cell density in the wound area expressed relative to the cell density outside of the wound area over time), in percentage, of MDCKII cells stably expressing inducible pLVX-GFP, pLVX-GFP ARHGEF2^{WT}, and pLVX-GFP ARHGEF2^{S151A} exposed to increasing amounts of doxycycline (Dox) at 6 and 18 hours. Bottom: Comparison of the wounds at 18 hours. Blue, mask of the original wound; orange, wound not closed. Data are means ± SD of three independent experiments done in triplicates. Statistical significance was determined by a two-way ANOVA test with a Bonferroni posttest correction for multiple comparisons. *P = 0.0445; **P = 0.0029; ****$P \leq$ 0.0001. NT, no treatment.

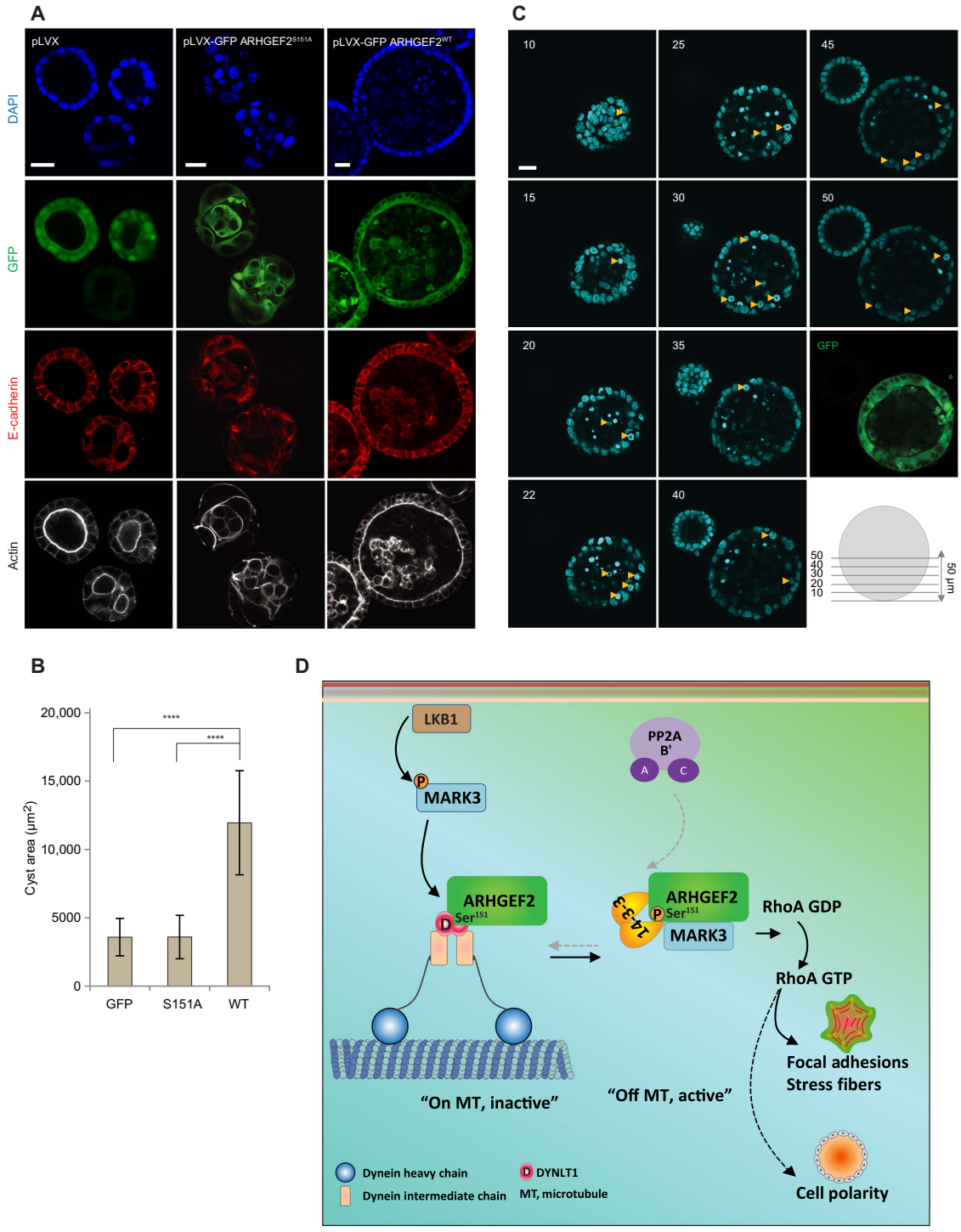

Fig. 8. Phosphorylation of ARHGEF2 Ser^{151} is required for normal cell polarity. (**A** to **C**) 3D culture of MDCKII cells stably expressing inducible pLVX-GFP, pLVX-GFP ARHGEF2^{WT}, and pLVX-GFP ARHGEF2^{S151A}. (A) GFP fluorescence was visualized and cysts were stained for E-cadherin, actin, and 4′,6-diamidino-2-phenylindole (DAPI). Scale bars, 20 µm. (B) Average size of the cysts observed in pLVX-GFP, pLVX-GFP ARHGEF2^{WT}, and pLVX-GFP ARHGEF2^{S151A} (n = 24, 21, and 24, respectively). Data are means ± SD of three independent experiments. Statistical significance was determined by a one-way ANOVA test with a Bonferroni posttest correction for multiple comparisons. ****$P \leq 0.0001$. (C) Z-stacks (1 µm) of pLVX-GFP ARHGEF2^{WT} cysts. Abnormal mitotic events are indicated (yellow arrows). Note that the cyst on the left has lost expression of pLVX-GFP ARHGEF2^{WT}. Numbers represent the Z-stack step. Images are representative of four independent experiments. Scale bar, 20 µm. (**D**) Model of MARK3- and PP2A-mediated regulation of ARHGEF2 phosphorylation and its effects on RHOA activation. LKB1 activates MARK3, which in turn phosphorylates ARHGEF2 on Ser^{151}. This creates a 14-3-3 binding site that disrupts ARHGEF2 interaction with DYNLT1 and releases it from microtubules to activate RHOA and trigger the formation of stress fibers and focal adhesions. MARK3-mediated phosphorylation of Ser^{151} is required for epithelial cell polarity in 3D growth. PP2A dephosphorylates Ser^{151} through interactions with the B′ subunits. GDP, guanosine diphosphate; GTP, guanosine triphosphate.

cellular effect of ARHGEF2 using the TETi system to titrate the concentrations of MARK3, ARHGEF2^{WT}, and ARHGEF2^{S151A} (fig. S6, A, D, and E). After induction with doxycycline, the cells were fixed and stained for vinculin and actin to assess the formation of focal adhesions and stress fibers, respectively (Fig. 7, A to D, and fig. S7). Induction of pLVX-GFP-ARHGEF2^{WT} strongly enhanced the formation of stress fibers and focal adhesions and led to a decreased rate in wound closure, likely due to enhanced adherence of the cells (Fig. 7, A to E, and fig. S7A). In contrast, the induction of pLVX-GFP-ARHGEF2^{S151A} produced significantly less stress fibers and focal adhesions and had little impact on wound healing rates compared to that of pLVX-GFP-ARHGEF2^{WT} (Fig. 7, A to E). The ability of ARHGEF2 to induce actin reorganization and focal adhesion formation was attenuated by silencing of *MARK3* with specific siRNA (Fig. 7, A to D). Consistent with these observations, induced expression of MARK3 promoted the formation of focal adhesions and stress fibers in a manner similar to ARHGEF2 (fig. S7, B to F). These data demonstrated a functional link between ARHGEF2 and MARK3 and showed that the ability of ARHGEF2 to induce polymerized actin structures was contingent on MARK3.

Phosphorylation of ARHGEF2 on Ser^{151} controls cell polarity

To determine the role of Ser^{151} phosphorylation in cell polarity, we grew transfected cells in three-dimensional (3D) culture. Cells expressing GFP alone initiated lumen formation at day 4, whereas those expressing GFP-ARHGEF2^{WT} had already established a well-defined lumen. In distinction, the pLVX-GFP-ARHGEF2^{S151A} cells failed to initiate the formation of proper 3D structures at day 4 (fig. S8A). After 8 days of growth in Matrigel, the pLVX-GFP control cells developed a spherical structure with a hollow lumen. Expression of GFP-ARHGEF2^{WT} led to larger spheroid structures with maintained polarity but with decreased luminal clearance of cells (Fig. 8, A and B). In contrast, expression of GFP-ARHGEF2^{S151A} led to smaller spheroids with disorganized arrangement of cells, which were unable to form polarized structures with well-defined lumen (Fig. 8, A and B).

Analysis of the distribution of the tight junction proteins zonula occludens 1 [ZO-1; also known as tight junction protein 1 (TJP1)] and ZO-2 (or TJP2) in 2D cultures revealed differences in the distribution of ZO-1 and ZO-2 between the control pLVX-GFP cells compared to that of the mutant pLVX-GFP-ARHGEF2^{S151A} (fig. S8B). The staining of ZO-1 and ZO-2 observed along cell junctions in control cells was disrupted in cells expressing GFP-ARHGEF2^{S151A}, particularly between adjacent cells, consistent with defective tight junction formation. On the other hand, GFP-ARHGEF2^{WT}–expressing cells showed an enhanced ZO-1 and ZO-2 signal at cell junctions compared to the control GFP (fig. S8B).

In 3D cultured cells, we observed a classical distribution of ZO-1 in the lumen of pLVX-GFP cells. This signal was strongly enhanced in pLVX-GFP-ARHGEF2^{WT} cells with an atypical distribution of the ZO-1 staining at the lumen and the periphery of the spheroid. In contrast, the ZO-1 signal in pLVX-GFP-ARHGEF2^{S151A} cells was attenuated (fig. S8C). These observations reinforce our claim that expression of ARHGEF2^{S151A} disturbs the normal sequence of cellular polarization required for epithelial cyst formation in 3D culture.

Multiple mitotic figures were evident in the polarized epithelial layer of the spheres in pLVX-GFP-ARHGEF2^{WT} cells, suggesting enhanced mitosis (Fig. 8C). We observed enhanced proliferation in spheroids formed by pLVX-GFP-ARHGEF2^{WT} cells (Ki67 staining), with some luminal cells positive for Ki67 (fig. S8D). Active caspase 3 was detected in subsets of those luminal cells (fig. S8E), showing that these cells were also undergoing cell death processes as well as proliferation.

These data demonstrate that ARHGEF2 contributed to spheroid size and the maintenance of epithelial polarity, whereas a mutant form of ARHGEF2 uncoupled from MARK3 interfered with the signaling program required to establish epithelial polarity and normal spheroid formation.

DISCUSSION

We used a proteomic approach to identify ARHGEF2 as a substrate of MARK3 and mapped a MARK3 phosphosite on Ser^{151} of ARHGEF2, which regulates the interaction of ARHGEF2 with the dynein motor light chain DYNLT1 through the creation of a 14-3-3 binding site. We solved a crystal structure of DYNLT1 in complex with an ARHGEF2 peptide comprising the binding site, which reveals that ARHGEF2 residues 140 to 155 lie in the groove formed at the interface of the two homodimeric DYNLT1 subunits. We showed that the phosphorylation of the Ser^{151} site per se was insufficient to disrupt this complex. Rather, phosphorylation of Ser^{151} created a higher-affinity 14-3-3 binding site, which antagonized ARHGEF2 binding to DYNLT1 through direct competition for the binding site. 14-3-3 proteins frequently regulate the intracellular localization of their target proteins by the masking of subcellular targeting sequences such as nuclear localization sequences. Occluding the binding site between a dynein (DYNLT1) and its cargo protein (ARHGEF2) represents a previously unknown mechanism of regulation of protein subcellular localization by 14-3-3 proteins (*45*, *74*, *75*). We also showed that PP2A restored the dephosphorylated state of Ser^{151} and thus returned it to the inactive state associated with the microtubule array. Consistent with this model, stress fiber formation is increased upon inhibition of PP2A family phosphatases with OA (*76*), which may be mediated through inhibition of ARHGEF2 dephosphorylation. Thus, phosphorylation of Ser^{151} served as a reversible switch leading to the displacement and activation of ARHGEF2 from the microtubule-associated dynein motor complex, and subsequent activation of RHOA, which affected 3D cell growth (Fig. 8D).

The release from microtubules and activation of ARHGEF2 can thus be regulated by three distinct modes. First, direct disruption of polymerized microtubules by pharmacologic agents such as nocodazole or colchicine releases ARHGEF2 and leads to potent activation of RHOA, an effect that can be reversed by the microtubule-stabilizing drug paclitaxel (*27*, *77*–*79*). Second, the G protein (heterotrimeric guanine nucleotide–binding protein)–coupled receptor (GPCR) ligands lysophosphatidic acid and thrombin trigger activation of ARHGEF2 through the disassembly of the ARHGEF2-dynein multiprotein complex by the concerted action of Gα and Gβγ. Gα binds directly to ARHGEF2 and displaces it from DYNLT1, while Gβγ binds to DYNLT1 and disrupts its interaction with the DIC, resulting in the release of ARHGEF2 from microtubules (*30*). Third, we showed here that the phosphorylation of the Ser^{151} regulatory site on the N terminus of ARHGEF2 by MARK3 disrupted its binding to DYNLT1 by creating a 14-3-3 binding site, triggering its release from the microtubule network and activation.

The identification of MARK3 as a kinase, which creates a 14-3-3 binding site on ARHGEF2, is consistent with a more general function of MARK family members in controlling substrate function or activity through the creation of 14-3-3 binding sites (*40*, *65*, *72*, *73*). The cell cycle–regulated phosphatase CDC25C is sequestered in the cytoplasm by MARK3-dependent phosphorylation and subsequent binding to 14-3-3. Similarly, phosphorylation of KSR1 by MARK3 creates a 14-3-3 binding site, which impairs its ability to translocate to the plasma membrane and fully activate the MAPK pathway.

ARHGEF2 can be stabilized in an active state when 14-3-3 is bound to phospho-Ser[151] in the N terminus or in an inactive state associated with polymerized microtubules when 14-3-3 is bound to phospho-Ser[885] in the C terminus. Similarly, RAF1 can be locked in an active or an inactive state by 14-3-3 binding to distinct C- or N-terminal sites, respectively. PP2A can also activate or inactivate RAF1 by differential dephosphorylation of these regulatory sites (*80*, *81*).

14-3-3 proteins recognize sites containing phosphorylated serine or threonine residues in the context of peptide sequences containing RSx(pS/pT)xP (mode I), RxF/Yx(pS/pT)xP (mode II) (*45*, *82*–*84*), or phosphosites at the penultimate C-terminal position [x(pS/pT)x-COOH] (*82*, *83*, *85*), as well as various noncanonical motifs. We suggest that the ARHGEF2 Ser[885] phosphosite contained within the sequence RRRpSLP is a high-affinity 14-3-3 binding site that conforms to the mode I motif, whereas the Ser[151] phosphosite contained within the sequence KSVpSTT is a lower-affinity suboptimal mode I sequence (http://scansite3.mit.edu/) (*86*) because it lacks the Pro residue that directs the C terminus of the peptide out of the binding cleft. A similar site that lacks proline at position +2 and has a lysine at position −3 instead of arginine was identified in the cytoplasmic tail of β_2 integrin, where phosphorylation of threonine within the sequence KSApTTT creates a binding site for 14-3-3, which competes with and displaces talin (*87*).

Further work will be required to understand the physiologic input that controls MARK3 activation. The MARK family of kinases includes four family members that regulate the cell cycle and cell polarity, and in turn, these kinases are phosphorylated and activated by LKB1 and aPKC (atypical protein kinase C) (*15*, *63*, *88*). MARK3 is constitutively active in cells (*89*), and how its kinase activity is regulated is not currently known. MARK3 is a multiply phosphorylated protein containing at least 17 phosphorylation sites identified in cells. Five MARK3 phosphorylation sites are followed by a proline residue, suggesting that they may be phosphorylated by proline-directed kinases, such as the MAPKs, CDKs (cyclin-dependent protein kinases), or GSK3 (glycogen synthase kinase 3) (*65*, *90*, *91*). Some of these sites represent 14-3-3 binding sites that may control the subcellular localization of MARK3, which is localized in the cytoplasm when phosphorylated and bound to 14-3-3, whereas a MARK3 mutant lacking all 17 known phosphorylation sites and unable to bind to 14-3-3 is enriched on the plasma membrane (*65*). The mechanism by which LKB1 activates MARK3 remains unknown. Both MARK2 and MARK3 maintain some activity in *LKB1*$^{-/-}$ mouse embryonic fibroblasts and LKB1-null HeLa cells (*63*), suggesting that other kinases may activate MARKs and contribute to the basal Ser[151] phosphorylation observed in *LKB1*-deficient A549 cells. Nevertheless, we have provided genetic and biochemical evidence that LKB1 stimulated ARHGEF2 Ser[151] phosphorylation by MARK3. Further work is required to determine how cell polarization affects the distribution and stoichiometry of MARK3 phosphorylation sites.

ARHGEF2 can interact with all four members of the MARK family and form a complex with the *H. pylori* bacterial oncoprotein CagA (*92*). MARK2 phosphorylates ARHGEF2 on Ser[885] and Ser[959], leading to the inhibition of the GEF activity with suppression of RHOA activation and stress fiber formation (*36*). MAPs MAP2, MAP4, and MAPT/TAU are substrates of MARKs (*93*–*95*), with an emerging role for MARK4 in the phosphorylation of MAPT/TAU in Alzheimer's disease (*96*). The identification of ARHGEF2 and other MAPs including CLASPs, which are involved in planar cell polarity in *Arabidopsis thaliana* by mediating the orientation of cell division planes in roots (*97*), as MARK3 substrates suggests that MARK3 is part of a protein network that regulates microtubule function and highlights the importance of the microtubule network in cell polarity. ARHGEF2 may be distinct from other MARK3 substrates linked to cell polarity in that the mutation of a single phosphosite leads to profound defects in 3D growth. Our results reflect the importance of the phosphorylation of Ser[151] in ARHGEF2 in controlling cell polarity in 3D growth in mammalian cells and are consistent with previous observations in which the lack of ARHGEF2 in *Xenopus* leads to severe defects in neuronal tube closure due to defects in polarity linked with alterations in myosin II light chain phosphorylation and accumulation of Rab11 and actin (*98*). ARHGEF2 interacts with ZO-2 in MDCK cells, and the lack of ZO-2 leads to an increase in RHOA activation mediated by ARHGEF2. The lack of ZO-2 also causes misorientation of the mitotic spindle and promotes the formation of multiple lumens in cysts in 3D culture, effects associated with RHOA and CDC42 activation (*99*).

Within this MARK3 interaction network, we also identified the PP2A regulatory subunit B alpha (PPP2R2A) and the scaffold subunit A alpha (PPP2R1A) as well as several tyrosine protein phosphatases (PTPN3, PTPN13, and PTPN14) that could influence microtubule dynamics in highly polarized epithelial cells. Because other members of the MARK family interact with ARHGEF2, we cannot exclude the possibility that they could also contribute to the regulation of cell polarity through ARHGEF2 (*92*).

ARHGEF2 is a multifunctional guanine exchange factor involved in RHOA activation and MAPK pathway activation through its noncatalytic scaffold function. We have uncovered a previously unknown phosphoregulatory switch, which regulates the subcellular localization and activity of ARHGEF2. The LKB1-MARK3 pathway and PP2A dynamically control the phosphorylation state of ARHGEF2 required for the establishment of cell polarity.

MATERIALS AND METHODS

Cell lines and cell culture

All cell lines were maintained in a 5% CO_2 environment at 37°C and grown in Dulbecco's modified Eagle's medium (DMEM; Invitrogen), supplemented with regular or tetracycline-free 10% fetal bovine serum (FBS) (WISENT Inc.) for the doxycycline-inducible cell lines. The following cell lines were used in this study: HEK293T (American Type Culture Collection), Cos cells; MDCKII (S. Muthuswamy, Beth Israel Deaconess Medical Center/Harvard Medical); and 293T-Rex cells expressing Flag-tagged PP2A and PP6 subunits and Flag-tagged GFP. Untransfected 293 Flp-In T-REx cells (Invitrogen) were additionally supplemented with zeocin (100 μg/ml) and blasticidin (5 μg/ml). After transfection and selection of stable lines expressing FlagBirA* alone or FlagBirA*-ARHGEF2, the cells were maintained with hygromycin B (100 μg/ml) according to the manufacturer's instructions.

Transfection

Plasmid DNAs were transfected into HEK293T and 293T-Rex cells using LipoD293 (SignaGen) according to the manufacturer's instructions. Transfected cells were kept for 24 to 48 hours in fully supplemented medium.

3D culture

An eight-well chambered cover glass system (Nunc Lab-Tek II, Thermo Fisher Scientific) was coated evenly with 50 μl of Matrigel matrix (Corning) per well and incubated at 37°C for 40 min to allow the matrix

to solidify. MDCKII cells were trypsinized and counted, and a total of 5×10^3 cells were resuspended in 400 µl of 3D culture medium [DMEM + 10% FBS + 2% Matrigel ± doxycycline (1 µg/ml)] and placed on top of the solidified matrix. The cells were allowed to grow for 4 or 8 days, with fresh 3D culture medium replenishment every 4 days.

Live imaging

HEK293T cells were seeded onto 24-well microplates (ibiTreat, Ibidi). Subconfluent cells were transfected as previously indicated, with pEGFP-C1 or pcDNA3 monomeric Cherry-tagged vectors. After 24 hours of transfection, live-cell imaging of HEK293T was performed on an inverted confocal microscope (Olympus IX81 inverted microscope) with a built-in incubator maintained in a 5% CO_2 environment at 37°C using a 60×/1.2 U-PlanApo water objective (Nikon) and FluoView software (Olympus).

GO, network, motif scan, and ARHGEF2 ortholog analysis

GO analysis of the network (*100*, *101*) was performed using all the interactors (http://geneontology.org). A further analysis, using the GO curated terms and literature reports, was done to manually classify six genes that remained unclassified (*ANKRD52, ANKRD28, CEP170, CEP170B*, *PPP6R2*, and *MTUS1*). The final network was built with Cytoscape_v3.1.0 (*102*) using shared interactions based on GeneMANIA (www.genemania.org/) (*103*). The motif scan was done using ScanProsite (http://prosite.expasy.org/scanprosite) (*104*, *105*) submitting the sequences of CLASP1 (Q7Z460), CLASP1 (O75122), and ARHGEF2 (Q92974) according to their UniProt Knowledgebase (UniProtKB) accession entries. ARHGEF2 orthologs were obtained using UniProtKB (www.uniprot.org) (*106*), and reviewed (marked with an asterisk in Fig. 2E) and unreviewed orthologs were selected for the analysis. The UniProtKB sequences were aligned using PRALINE (PRofile ALIgNEment) (www.ibi.vu.nl/programs/pralinewww/) (*107*, *108*).

Immunoblots and coimmunoprecipitation assays

Cells were lysed in NP-40 lysis buffer as previously described (*73*) to analyze interactions with MARK3. Triton X-100 lysis buffer (50 mM Hepes, 150 mM NaCl, 1% Triton X-100, 10% glycerol, 1 mM EGTA, 1 mM EDTA, and protease and phosphatase inhibitors; Thermo Fisher Scientific) was used to analyze interactions with PP2A and PP6 subunits. After the indicated treatment or transfection, the cells were washed once in cold phosphate-buffered saline (PBS) and lysed for 20 min on ice. After centrifugation at 13,000 rpm for 10 min at 4°C, cleared lysates were directly resolved by SDS-PAGE by boiling in Laemmli sample buffer for 5 min and analyzed by Western blotting or the protein complexes were incubated with antibodies overnight to immunoprecipitate endogenous proteins for 1 hour at 4°C with anti-Flag M2 affinity gel to immunoprecipitate Flag-tagged proteins or an antibody against GFP. After the incubation period, protein A–agarose (Roche) for GFP immunoprecipitates or protein G agarose (BioShop) for endogenous immunoprecipitates was added, and the mixture was incubated for an additional hour at 4°C. The beads were pelleted and washed three times with cold lysis buffer. Samples were processed for SDS-PAGE by boiling in 2× Laemmli sample buffer and analyzed by Western blotting. Quantifications were performed using the ImageJ 1.37c software and were representative of three independent experiments unless indicated otherwise.

Immune complex kinase assays

Plasmid DNAs encoding hemagglutinin (HA)–tagged CLASP1, CLASP2, or ARHGEF2 were transfected into Cos cells using the FuGENE reagent (Roche). Forty-eight hours after transfection, Cos cells were lysed under stringent conditions using radioimmunoprecipitation assay (RIPA) buffer (NP-40 lysis buffer containing 0.5% sodium deoxycholate and 0.1% SDS). HA-tagged CLASP1, CLASP2, or ARHGEF2 proteins were immunoprecipitated from cell lysates, following which the immune complexes were washed three times with NP-40 lysis buffer and once with 30 mM tris (pH 7.4). The complexes were then resuspended in 40 µl of kinase buffer [30 mM tris (pH 7.4), 1 mM dithiothreitol (DTT), 10 mM $MgCl_2$, 5 mM $MnCl_2$, and 1 µM ATP] containing 20 µCi of [γ-^{32}P]ATP and 0.2 µg of either purified MARK3^{WT} or a kinase-deficient MARK3^{KD} mutant and incubated at 30°C for 30 min. The assays were terminated by the addition of gel sample buffer [250 mM tris (pH 6.8), 50 mM DTT, 10% SDS, and 30% glycerol]. Samples were resolved by SDS-PAGE, and the phosphoproteins were visualized by autoradiography.

Metabolic labeling of cells

Cos cells expressing HA-tagged ARHGEF2 were incubated for 4 to 6 hours at 37°C in phosphate-free DMEM containing 2.5% dialyzed calf serum and 1 mCi of [^{32}P]orthophosphate per milliliter of labeling medium. Cells were then washed twice with ice-cold tris-buffered saline [20 mM tris (pH 7.4) and 137 mM NaCl] and lysed in RIPA buffer. ARHGEF2 proteins were immunoprecipitated from cell lysates and washed extensively with NP-40 lysis buffer. Samples were examined by SDS-PAGE and autoradiography.

Phosphorylation site mapping

^{32}P-labeled proteins were eluted from the SDS-PAGE gel matrix, precipitated using trichloroacetic acid, and digested with trypsin. An aliquot of the digested protein was adjusted to pH 2 with 20% trifluoroacetic acid and loaded onto a Waters 3.9 mm by 300 mm C_{18} column. Reversed-phase HPLC was performed in an LKB chromatography system with two 2150 HPLC pumps, a 2152 LC controller, and a 2140 rapid spectral detector. When buffer salts began to elute, an increasing gradient of acetonitrile in 0.05% aqueous trifluoroacetic acid was added to the column. The stepwise gradient at a flow rate of 1 ml/min was 0 to 40% CH_3CN for 60 min, 40% CH_3CN for 10 min, 40 to 60% CH_3CN for 10 min, and 60% CH_3CN for 10 min. Fractions were collected at 1-min intervals, and ^{32}P content was determined by measuring Cerenkov counts. HPLC fractions containing peaks of radioactivity were subjected to phosphoamino analysis and semiautomated Edman degradation in a spinning-cup sequenator, as previously described (*109*).

Generation of stable TETi cell lines

Stable cells expressing GFP, MARK3, ARHGEF2, GFP-tagged ARHGEF2^{WT}, and GFP-tagged ARHGEF2^{S151A} under the control of a TETi promoter were generated using the lentiviral Tet-On 3G Inducible Expression System (Clontech). Lentiviral particles were generated in HEK293T by cotransfection of the viral vectors with packaging and envelope plasmids (pPAX2 and VSV-g) using X-tremeGENE as previously described (*26*). Stable doxycycline-inducible MDCKII cells were established by cotransduction with two lentiviral vectors according to the manufacturer's instructions (Clontech): a regulator vector that stably expresses the Tet-On 3G transactivator protein and a second vector that contains the TRE3G promoter controlling the expression of untagged MARK3 or ARHGEF2 in a 1:1 ratio (see fig. S6A for details). The cells were selected with puromycin (10 µg/ml; BioShop) and G418 (200 µg/ml; BioShop) and maintained in DMEM + 10% FBS

(tetracycline-free; WISENT Inc.) after antibiotic selection. Nontransduced cells were used to determine the optimal concentration of antibiotic for selection.

Antibodies and reagents

Western blotting, immunoprecipitation, and immunofluorescence were performed using the following antibodies: an antibody recognizing the Pyo-derived epitope tag, which has been reported previously (*110*); antibodies recognizing MARK3 and vinculin (immunofluorescence) (Millipore); and antibodies against Flag (clone M2, Sigma) and HA (Covance). To detect endogenous ARHGEF2, we used a mouse monoclonal antibody (clone 3C5) designed using N-terminal human ARHGEF2 peptides and produced by hybridoma as previously described (*26*) and an antibody recognizing a region within amino acids 656 to 1000 of human ARHGEF2 (ab155785, Abcam). For endogenous immunoprecipitation of ARHGEF2, we used the ARHGEF2-specific antibody A301-929A (Bethyl); antibodies recognizing 14-3-3 (all isoforms), Myc (9E10), α-tubulin, and ZO-2 (immunofluorescence) (Santa Cruz Biotechnology); antibodies recognizing ERK1/2, pARHGEF2 Ser^{886}, pARHGEF2 Ser^{151} (custom-produced), AMPKα, pAMPKα Thr^{172}, LKB1, GAPDH, and cleaved caspase 3 (immunofluorescence) (Cell Signaling); Alexa Fluor 647 phalloidin (Thermo Fisher Scientific); antibody specific for ZO-1 (Life Technologies); and antibody specific for Ki67 (immunofluorescence) (Abcam). The following reagents were used: AICAR (Santa Cruz Biotechnology) and OA (BioShop). For siRNA treatments, Lipofectamine RNAiMAX (Thermo Fisher Scientific) was used to transfect 10 nM predesigned siRNA control or *MARK3* s230619 and s69595 (Silencer Select, Thermo Fisher Scientific).

Expression constructs

Full-length, truncated, and mutated human ARHGEF2 constructs (NM_001162384.1) were cloned into the 3XFlag pCMV.10 vector (Sigma), pEGFP-C1 (Clontech), or pcDNA3.1/myc-His(−)B (Invitrogen) and verified by sequencing. Bovine DYNLT1 (accession no. NM_174620) and murine 14-3-3ζ (YWHAZ) were cloned into 3XFlag pCMV.10 or pGEX-4T-3 vectors for recombinant protein generation, as previously described (*28*). pcDNA3 constructs encoding pyo-KSR1 N′424 (residues 1 to 424) and full-length pcDNA3-Pyo-$MARK3^{WT}$ and pcDNA3-Pyo-$MARK3^{KD}$ (kinase-deficient) have been previously described (*40*, *110*). In addition, full-length ARHGEF2 and MARK3 were cloned into the TREG vector (Clontech) and into pcDNA3 monomeric Cherry vectors. Point mutations were introduced by site-directed mutagenesis (QuikChange, Stratagene), and deletions were introduced by designing forward and reverse primers flanking the region to be deleted (Q5 Site-Directed Mutagenesis Kit, New England Biolabs Inc.).

For structural analyses of DYNLT1, a pGEX-4T-1 expression vector containing full-length murine DYNLT1 complementary DNA (cDNA) was a gift from M. Zhang (Hong Kong University of Science and Technology). Murine ARHGEF2 (AF177032) constructs [residues 136 to 161 and 136 to 164 and a variant of 136 to 161 with a cysteine substitution (Cys^{136})] were generated by annealing DNA oligomers with Bam HI and Eco RI compatible overhangs, which were ligated into a digested pGEX-4T-1 vector to encode thrombin-cleavable GST-fused fragments. A chimeric construct of ARHGEF2 residues 136 to 164 fused to the C terminus of DYNLT1 through a linker of sequence GLEGGSGGSG was generated by amplifying the ARHGEF2 region with primers encoding the additional linker sequence flanked by Xho I restriction sites. The TGA stop codon of DYNLT1 in the pGEX-4T-1 expression vector was mutated to GGA using QuikChange, and the vector and polymerase chain reaction (PCR) product were each digested by Xho I, ligated together, and screened for correct orientation by Sanger sequencing. The linker sequence was subsequently shortened to a single glycine using QuikChange.

Protein expression for structural analysis

Escherichia coli BL21(DE3) CodonPlus-RIL (Agilent) cells were transformed with DYNLT1, DYNLT1:ARHGEF2 chimera, or murine ARHGEF2 constructs and grown overnight in lysogeny broth medium supplemented with chloramphenicol (50 μg/ml) and ampicillin (100 μg/ml) at 37°C while shaking. These cells were pelleted by centrifugation and transferred into fresh lysogeny broth for expression of unlabeled protein or M9 medium supplemented with [^{15}N]ammonium chloride (1 g/liter) and/or [^{13}C]glucose (2 g/liter) to produce isotopically labeled (^{13}C and/or ^{15}N) DYNLT1 or DYNLT1:ARHGEF2 chimera. Protein expression was induced by adding 250 μM isopropyl-β-D-1-thiogalactopyranoside when the optical density at 600 nm of the culture reached ~0.8. The temperature was decreased to 15°C, and protein expression continued for about 19 hours. The cells were harvested by centrifugation, and the cell pellets were flash-frozen and stored at −70°C until purification.

Protein and peptide purification

Frozen BL21 cell pellets expressing DYNLT1 or DYNLT1:ARHGEF2 chimera were thawed on ice and resuspended in lysis buffer [50 mM tris-HCl (pH 8.0), 300 mM NaCl, 0.5 mM EDTA (pH 8.0), 0.1% NP-40, and 2 mM DTT]. Cells were lysed by sonication, and the cell debris was removed by centrifugation. Glutathione Sepharose 4B resin (GE Healthcare Life Sciences) was mixed with the supernatant and incubated at 4°C for 1 hour. The resin was extensively washed with a high-salt buffer 1 [50 mM tris-HCl (pH 8.0), 300 mM NaCl, and 2 mM DTT] followed by a lower-salt buffer 2 [50 mM tris-HCl (pH 8.0), 150 mM NaCl, and 2 mM DTT]. The resin was resuspended, and DYNLT1 was cleaved from the GST tag by thrombin (10 U/mg of bound protein) for 48 hours at 4°C and then further purified on a Superdex 75 26/60 size exclusion column (GE Healthcare Life Sciences) run with 50 mM tris-HCl (pH 7.0), 400 mM KCl, and 2 mM DTT. Fractions containing pure DYNLT1 or DYNLT1:ARHGEF2 were collected and concentrated for NMR and crystallographic studies. ARHGEF2 peptides were purified in a similar manner using the following buffers: lysis buffer [50 mM tris-HCl (pH 7.5), 150 mM NaCl, 10% glycerol, 10 mM β-mercaptoethanol, and 0.1% NP-40], wash buffer 1 [50 mM tris-HCl (pH 7.5), 500 mM NaCl, 10% glycerol, and 10 mM β-mercaptoethanol], and wash buffer 2 [50 mM tris-HCl (pH 7.5), 150 mM NaCl, 10% glycerol, and 10 mM β-mercaptoethanol], and size exclusion chromatography was performed using a Superdex Peptide 10/300 GL column (GE Healthcare Life Sciences) run with 50 mM tris-HCl (pH 7.0), 100 mM KCl, and 0.2 mM tris(2-carboxyethyl)phosphine (TCEP). Peptide concentrations were calculated by the absorbance at 214 nm using a JASCO spectrophotometer, and purity was determined by silver staining (Invitrogen) tris-tricine SDS-PAGE gels.

NMR spectroscopy

2D ^{1}H-^{15}N HSQC spectra of 0.2 to 0.3 mM samples were acquired on Bruker Avance III 600-MHz and Bruker Avance II 800-MHz spectrometers at 25°C in a buffer consisting of 50 mM tris-HCl (pH 7.0), 100 mM KCl, 2 mM DTT, and 10% D_2O. 3D spectra (HNCA, HNCOCA, CBCACONH, HNCACB, HNCO, HNCACO, and NOE spectroscopy) for backbone assignments of the DYNLT1:ARHGEF2 chimera were acquired on 0.3 mM samples at 800 MHz in 50 mM phosphate buffer

(pH 6.7), 400 mM KCl, 2 mM DTT, and 10% D_2O at 35°C. NMR data were processed with NMRDraw and NMRPipe (*111*), whereas spectra were analyzed with NMRView (*82*).

Paramagnetic relaxation enhancement

ARHGEF2 peptides (residues 137 to 158) were synthesized with an additional cysteine at either the N terminus or C terminus (LifeTein) and a tryptophan at the opposite terminus to enable quantification by 280-nm ultraviolet absorption. Peptides were conjugated to a maleimide-linked EDTA tag (Toronto Research Chemicals) overnight at room temperature in the presence of 0.2 mM TCEP, and then either paramagnetic Mn^{2+} ($MnCl_2$) or diamagnetic Ca^{2+} ($CaCl_2$) was added. After 2 hours, excess metal ions and unconjugated tag were removed by dialysis against 25 mM Hepes (pH 7), 100 mM KCl, and 0.2 mM TCEP overnight at room temperature. Spectral perturbations of ^{15}N-labeled DYNLT1 induced by the addition of the ARHGEF2 peptides bound to Ca^{2+} or Mn^{2+} ions were compared to localize the N terminus of the peptide through additional peak broadening associated with the conjugated paramagnetic Mn^{2+}.

Crystallography

The DYNLT1:ARHGEF2 chimera with the optimized single glycine linker was crystallized at a protein concentration of 400 μM in a hanging drop by the vapor diffusion method using a buffer composed of 2.33 M ammonium sulfate [$(NH_4)_2SO_4$], 0.25 mM sodium malonate (pH 7) ($C_3H_2O_4Na_2$), and 7.2 mM $CaCl_2$. Crystals were allowed to grow for a few weeks, then harvested, soaked in 1 M sodium malonate (pH 7) as a cryoprotectant (*112*), and flash-frozen in liquid nitrogen. Diffraction and data collection were performed at the synchrotron x-ray source (Advanced Photon Source at Argonne National Laboratory), and phasing was solved by molecular replacement using the Drosophila DYNLT1 structure (PDB: 1YGT). Flexible portions of the structure were deleted, whereas nonconserved residues were modified to alanines.

MST and fluorescence polarization

Four 16-mer ARHGEF2 peptides comprising amino acids 876 to 891 with and without the phosphorylation of Ser^{885} (RRPLDPRRR[(p)Ser^{885}]LPAGDA[Lys(FITC)]) and amino acids 142 to 157 with and without the phosphorylation of Ser^{151} (SSLSLAKSV[(p)Ser^{151}]TTNIAG[Lys(FITC)]) were synthesized with a C-terminal FITC fluorescent tag (Biomatik Corp.). 14-3-3 protein was expressed as a recombinant GST fusion protein and purified by glutathione Sepharose followed by size exclusion chromatography. The affinity between these ARHGEF2 peptides and 14-3-3 protein was measured by MST (Monolith NT.115, NanoTemper) by preparing a series of standard MST glass capillaries containing each fluorescent peptide (100 nM) and increasing concentrations of GST–14-3-3 (serial dilutions from 195 μM to 2 nM) in 20 mM Hepes (pH 7.4), 150 mM NaCl, 1 mM DTT, and 0.05% Tween 20. Data were analyzed using the NanoTemper analysis software package. To investigate the effect of Ser^{151} phosphorylation on binding of DYNLT1, a series of samples containing 10 nM ARHGEF2 peptides (residues 142 to 157 with and without Ser^{151} phosphorylation) and increasing concentrations of GST-DYNLT1 (serial dilutions from 1.15 mM to 70 nM) were analyzed by fluorescence polarization using a Molecular Devices SpectraMax M5. Although K_d values could not be determined because the binding curves did not reach saturation, phosphorylation had no appreciable effect on the binding curve.

BioID

BioID (*31*) was performed as previously described (*32*). In this assay, the promiscuous mutant biotin ligase BirA* ($BirA^{R118G}$) is expressed as a fusion with the protein of interest such that it will biotinylate interacting and proximal proteins, which can then be identified by affinity purification and MS. Full-length human ARHGEF2 (NM_001162384.1) was amplified by PCR using specific primers (forward, 5′-GGCGCGCCACCATGTCTCGGATCGAATCCCTC-3′; reverse, 5′-AGTTAGGCGGCCGCTTAGCTCTCGGAGGCTACAGC-3′) and cloned into the pcDNA5 FRT/TO FlagBirA* expression vector using Asc I and Not I restriction enzymes. Using the Flp-In system (Invitrogen), 293 Flp-In T-REx cells stably expressing FlagBirA* alone or the FlagBirA*-ARHGEF2 fusion were generated. After selection [DMEM + 10% FBS + hygromycin B (200 μg/ml)], subconfluent cells were incubated overnight in complete medium supplemented with tetracycline (1 μg/ml; Sigma) and 50 μM biotin (BioShop). Cells were collected and pelleted (2000 rpm for 3 min), and the pellets were washed twice with PBS, dried, and snap-frozen.

Biotin-streptavidin affinity purification for MS

The cell pellets were resuspended in 10 ml of lysis buffer [50 mM tris-HCl (pH 7.5), 150 mM NaCl, 1 mM EDTA, 1 mM EGTA, 1% Triton X-100, 0.1% SDS, 1:500 protease inhibitor cocktail (Sigma-Aldrich), and 1:1000 TurboNuclease (Accelagen)] and incubated on an end-over-end rotator at 4°C for 1 hour, briefly sonicated to disrupt any visible aggregates, and then centrifuged at 16,000*g* for 30 min at 4°C. The supernatant was transferred to a fresh 15-ml conical tube. Thirty microliters of packed, preequilibrated streptavidin Sepharose beads (GE Healthcare Life Sciences) was added, and the mixture was incubated for 3 hours at 4°C with end-over-end rotation. Beads were pelleted by centrifugation at 2000 rpm for 2 min and transferred with 1 ml of lysis buffer to a fresh Eppendorf tube. Beads were washed once with 1 ml of lysis buffer and twice with 1 ml of 50 mM ammonium bicarbonate (pH 8.3). Beads were transferred in ammonium bicarbonate to a fresh centrifuge tube and washed two more times with 1 ml of ammonium bicarbonate buffer. Tryptic digestion was performed by incubating the beads with 1 μg of MS-grade tosyl phenylalanyl chloromethyl ketone (TPCK)–treated trypsin (Promega) dissolved in 200 μl of 50 mM ammonium bicarbonate (pH 8.3) overnight at 37°C. The following morning, an additional 0.5 μg of trypsin was added and the beads were incubated for two additional hours at 37°C. Beads were pelleted by centrifugation at 2000*g* for 2 min, and the supernatant was transferred to a fresh Eppendorf tube. Beads were washed twice with 150 μl of 50 mM ammonium bicarbonate, and these washes were pooled with the first eluate. The sample was lyophilized and resuspended in buffer A (0.1% formic acid). Each MS analysis was performed on an aliquot of one-fifth of this sample.

Mass spectrometry

MS was performed as previously described (*34*). Briefly, analytical columns (inner diameter, 75 μm) and precolumns (inner diameter, 150 μm) were made in-house from fused silica capillary tubing (InnovaQuartz) and packed with 100 Å C_{18}-coated silica particles (Magic, Michrom BioResources). Peptides were subjected to LC–electrospray ionization–MS/MS using a 120-min reversed-phase (100% water–100% acetonitrile, 0.1% formic acid) buffer gradient running at 250 nl/min on a Proxeon EASY-nLC pump in-line with a hybrid LTQ Orbitrap Velos mass spectrometer (Thermo Fisher Scientific). A parent ion scan was performed in the Orbitrap using a resolving power of 60,000, and then the most intense peaks (up to 20) were selected for MS/MS (minimum ion count of 1000 for activation) using standard collision-induced dissociation fragmentation.

Fragment ions were detected in the LTQ. A dynamic exclusion protocol was activated such that MS/MS spectra of the same *m/z* (mass/charge ratio) (within a range of 15 ppm; exclusion list size equal to 500) detected twice within 15 s were excluded from analysis for 30 s. For protein identification, Thermo.RAW files were converted to the .mzXML format using ProteoWizard (*113*) and then searched using X!Tandem (*114*) against the human (Human RefSeq Version 45) database. X!Tandem search parameters were as follows: parent mass error, 15 ppm; fragment mass error, 0.4 Da; complete modifications, none; cysteine modifications, none; and potential modifications, +16@M and W, +32@M and W, +42@N terminus, and +1@N and Q. Data were analyzed using the trans-proteomic pipeline (*115*, *116*) via the ProHits software suite (*117*). Proteins identified with a Protein Prophet cutoff of 0.9 and at least two unique peptides were analyzed with the SAINT (significance analysis of interactome) express algorithm (v3.3) (*118*). Fourteen control runs (consisting of 14 FlagBirA* only) were collapsed to the three highest spectral counts for each prey. A Bayesian false discovery rate of 0.02 or higher, corresponding to a SAINT score of ≥0.79, was used to identify the bona fide interactors (*119*). The interactions are from two independent biological replicates of FlagBirA*-ARHGEF2 (denoted as "A" and "B").

Isolation of MARK3 complexes and MS analysis

The experiment was performed as previously described (*60*) using cycling Cos cells expressing Pyo-tagged MARK3^{WT}.

Immunofluorescence

For immunofluorescence imaging, subconfluent MDCKII cells were seeded on sterile Nunc Lab-Tek II chambered cover glass and treated the following day with doxycycline (10 to 500 ng/ml; Bio Basic Canada Inc.) or DMSO only as indicated for 18 to 24 hours. The cells were washed once with 1× PBS and visualized directly for live imaging or fixed with 4% paraformaldehyde at room temperature for 15 or 20 min for 3D culture cells. After fixation, the cells were washed three times with 1× PBS and permeabilized with 0.1% Triton X-100 for 10 to 15 min at room temperature, washed three times with 1× PBS, and blocked with 1× PBS, 1% bovine serum albumin (BSA), 0.1% Triton X-100, and 5% normal goat serum for 1 hour at room temperature. After blocking, the cover glass chambers were incubated at 4°C overnight with antibody specific for vinculin (Millipore) and diluted (1:300) in 1× PBS, 1% BSA, and 0.1% Triton X-100 at room temperature for 2 hours for 3D culture with an antibody against E-cadherin (1:1000; BD Biosciences). For the ZO-1, ZO-2, cleaved caspase 3 (diluted 1:100), and Ki67 (1:200) staining, the spheroids were permeabilized with 0.5% Triton X-100 for 15 min at room temperature, and the incubation with the primary antibody was done overnight at room temperature. After incubation with primary antibodies, the chambers were washed three times in 1× PBS and incubated with antibodies against mouse IgG (H+L) cross-adsorbed secondary antibody conjugated to Alexa Fluor 488, 568, or 647 (Invitrogen) and/or Alexa Fluor 647 phalloidin (1:50) for actin staining for 1 hour at room temperature. After incubation with the secondary antibody, the chambers were washed three times in 1× PBS, and if required, the nuclei were stained with DAPI (Molecular Probes, Invitrogen) for 10 min followed by two additional washes with 1× PBS. Confocal imaging was performed with an Olympus IX81 inverted microscope using a 60×/1.4 PlanApo oil or a 60×/1.20 water (Nikon) objectives.

Statistical analyses

Values are expressed as means, and error bars represent means ± SD. Statistical comparisons were made with Prism version 6.0e (GraphPad), and specific tests are indicated for each figure, where a statistical analysis was performed. All the tests were two-sided. A P value of ≤0.05 was considered statistically significant. Bonferroni adjustment was conducted to adjust for multiple comparisons for most of the tests.

SUPPLEMENTARY MATERIALS

www.sciencesignaling.org/cgi/content/full/10/503/eaan3286/DC1

Fig. S1. ARHGEF2 interaction network.
Fig. S2. Full alignment of ARHGEF2 orthologs in vertebrates.
Fig. S3. Quantitative analysis of the effect of MARK3 phosphorylation of ARHGEF2 on its interactions with DYNLT1 and 14-3-3.
Fig. S4. Structural characterization of the DYNLT1-ARHGEF2 interaction.
Fig. S5. MARK3, but not PP6, regulates the phosphorylation of ARHGEF2 Ser^{151}.
Fig. S6. Generation and validation of inducible cells.
Fig. S7. MARK3 affects the biological activity of ARHGEF2.
Fig. S8. Phosphorylation of ARHGEF2 Ser^{151} is required for normal cell polarity.
Table S1. Summary of ARHGEF2 interactors reported in this study.
Table S2. GO enrichment analysis of the ARHGEF2 network.
Table S3. Functional annotation of ARHGEF2 interactors.
Table S4. Analysis of MARK3–C-TAK1 complexes.
Table S5. Data collection and refinement statistics for the DYNLT1:ARHGEF2 chimera (PDB: 5WI4).
Data file S1. Raw data for the ARHGEF2 interactors reported in this study.

REFERENCES AND NOTES

1. S. Guo, K. J. Kemphues, *par-1*, a gene required for establishing polarity in *C. elegans* embryos, encodes a putative Ser/Thr kinase that is asymmetrically distributed. *Cell* **81**, 611–620 (1995).
2. P. Tomancak, F. Piano, V. Riechmann, K. C. Gunsalus, K. J. Kemphues, A. Ephrussi, A *Drosophila melanogaster* homologue of *Caenorhabditis elegans par-1* acts at an early step in embryonic-axis formation. *Nat. Cell Biol.* **2**, 458–460 (2000).
3. N. J. Bright, C. Thornton, D. Carling, The regulation and function of mammalian AMPK-related kinases. *Acta Physiol.* **196**, 15–26 (2009).
4. K. J. Kemphues, J. R. Priess, D. G. Morton, N. Cheng, Identification of genes required for cytoplasmic localization in early *C. elegans* embryos. *Cell* **52**, 311–320 (1988).
5. D. N. Cox, B. Lu, T.-Q. Sun, L. T. Williams, Y. N. Jan, *Drosophila par-1* is required for oocyte differentiation and microtubule organization. *Curr. Biol.* **11**, 75–87 (2001).
6. G. Drewes, A. Ebneth, U. Preuss, E.-M. Mandelkow, E. Mandelkow, MARK, a novel family of protein kinases that phosphorylate microtubule-associated proteins and trigger microtubule disruption. *Cell* **89**, 297–308 (1997).
7. B. Trinczek, M. Brajenovic, A. Ebneth, G. Drewes, MARK4 is a novel microtubule-associated proteins/microtubule affinity-regulating kinase that binds to the cellular microtubule network and to centrosomes. *J. Biol. Chem.* **279**, 5915–5923 (2004).
8. Y. M. Chen, Q. J. Wang, H. S. Hu, P. C. Yu, J. Zhu, G. Drewes, H. Piwnica-Worms, Z. G. Luo, Microtubule affinity-regulating kinase 2 functions downstream of the PAR-3/PAR-6/atypical PKC complex in regulating hippocampal neuronal polarity. *Proc. Natl. Acad. Sci. U.S.A.* **103**, 8534–8539 (2006).
9. J. Biernat, Y.-Z. Wu, T. Timm, Q. Zheng-Fischhöfer, E. Mandelkow, L. Meijer, E.-M. Mandelkow, Protein kinase MARK/PAR-1 is required for neurite outgrowth and establishment of neuronal polarity. *Mol. Biol. Cell* **13**, 4013–4028 (2002).
10. F. Lazaro-Diéguez, D. Cohen, D. Fernandez, L. Hodgson, S. C. van Ijzendoorn, A. Müsch, Par1b links lumen polarity with LGN–NuMA positioning for distinct epithelial cell division phenotypes. *J. Cell Biol.* **203**, 251–264 (2013).
11. N. A. Ducharme, C. M. Hales, L. A. Lapierre, A.-J. Ham, A. Oztan, G. Apodaca, J. R. Goldenring, MARK2/EMK1/Par-1Bα phosphorylation of Rab11-family interacting protein 2 is necessary for the timely establishment of polarity in Madin-Darby canine kidney cells. *Mol. Biol. Cell* **17**, 3625–3637 (2006).
12. J. K. Lennerz, J. B. Hurov, L. S. White, K. T. Lewandowski, J. L. Prior, G. J. Planer, R. W. t. Gereau, D. Piwnica-Worms, R. E. Schmidt, H. Piwnica-Worms, Loss of Par-1a/MARK3/C-TAK1 kinase leads to reduced adiposity, resistance to hepatic steatosis, and defective gluconeogenesis. *Mol. Cell. Biol.* **30**, 5043–5056 (2010).
13. C. Sun, L. Tian, J. Nie, H. Zhang, X. Han, Y. Shi, Inactivation of MARK4, an AMP-activated protein kinase (AMPK)-related kinase, leads to insulin hypersensitivity and resistance to diet-induced obesity. *J. Biol. Chem.* **287**, 38305–38315 (2012).
14. J. B. Hurov, M. Huang, L. S. White, J. Lennerz, C. S. Choi, Y.-R. Cho, H.-J. Kim, J. L. Prior, D. Piwnica-Worms, L. C. Cantley, J. K. Kim, G. I. Shulman, H. Piwnica-Worms, Loss of the Par-1b/MARK2 polarity kinase leads to increased metabolic rate, decreased adiposity, and insulin hypersensitivity in vivo. *Proc. Natl. Acad. Sci. U.S.A.* **104**, 5680–5685 (2007).

15. J. B. Hurov, J. L. Watkins, H. Piwnica-Worms, Atypical PKC phosphorylates PAR-1 kinases to regulate localization and activity. *Curr. Biol.* **14**, 736–741 (2004).
16. O. Akchurin, Z. Du, N. Ramkellawan, V. Dalal, S. H. Han, J. Pullman, A. Müsch, K. Susztak, K. J. Reidy, Partitioning-defective 1a/b depletion impairs glomerular and proximal tubule development. *J. Am. Soc. Nephrol.* **27**, 3725–3737 (2016).
17. I. Saadat, H. Higashi, C. Obuse, M. Umeda, N. Murata-Kamiya, Y. Saito, H. Lu, N. Ohnishi, T. Azuma, A. Suzuki, S. Ohno, M. Hatakeyama, *Helicobacter pylori* CagA targets PAR1/MARK kinase to disrupt epithelial cell polarity. *Nature* **447**, 330–333 (2007).
18. J. Howard, A. A. Hyman, Microtubule polymerases and depolymerases. *Curr. Opin. Cell Biol.* **19**, 31–35 (2007).
19. H. Bowne-Anderson, A. Hibbel, J. Howard, Regulation of microtubule growth and catastrophe: Unifying theory and experiment. *Trends Cell Biol.* **25**, 769–779 (2015).
20. J. Teng, Y. Takei, A. Harada, T. Nakata, J. Chen, N. Hirokawa, Synergistic effects of MAP2 and MAP1B knockout in neuronal migration, dendritic outgrowth, and microtubule organization. *J. Cell Biol.* **155**, 65–76 (2001).
21. X. Chen, X. Zhou, T.-C. Mao, X.-H. Shi, D.-L. Fan, Y.-M. Zhang, Effect of microtubule-associated protein-4 on epidermal cell migration under different oxygen concentrations. *J. Dermatol.* **43**, 674–681 (2016).
22. Y.-Y. Jiang, L. Shang, Z.-Z. Shi, T.-T. Zhang, S. Ma, C.-C. Lu, Y. Zhang, J.-J. Hao, C. Shi, F. Shi, X. Xu, Y. Cai, X.-M. Jia, Q.-M. Zhan, M.-R. Wang, Microtubule-associated protein 4 is an important regulator of cell invasion/migration and a potential therapeutic target in esophageal squamous cell carcinoma. *Oncogene* **35**, 4846–4856 (2016).
23. G. Benais-Pont, A. Punn, C. Flores-Maldonado, J. Eckert, G. Raposo, T. P. Fleming, M. Cereijido, M. S. Balda, K. Matter, Identification of a tight junction-associated guanine nucleotide exchange factor that activates Rho and regulates paracellular permeability. *J. Cell Biol.* **160**, 729–740 (2003).
24. E. Kakiashvili, P. Speight, F. Waheed, R. Seth, M. Lodyga, S. Tanimura, M. Kohno, O. D. Rotstein, A. Kapus, K. Szaszi, GEF-H1 mediates tumor necrosis factor-α-induced Rho activation and myosin phosphorylation: Role in the regulation of tubular paracellular permeability. *J. Biol. Chem.* **284**, 11454–11466 (2009).
25. A. A. Birukova, P. Fu, J. Xing, B. Yakubov, I. Cokic, K. G. Birukov, Mechanotransduction by GEF-H1 as a novel mechanism of ventilator-induced vascular endothelial permeability. *Am. J. Physiol. Lung Cell. Mol. Physiol.* **298**, L837–L848 (2010).
26. J. Cullis, D. Meiri, M. J. Sandi, N. Radulovich, O. A. Kent, M. Medrano, D. Mokady, J. Normand, J. Larose, R. Marcotte, C. B. Marshall, M. Ikura, T. Ketela, J. Moffat, B. G. Neel, A.-C. Gingras, M.-S. Tsao, R. Rottapel, The RhoGEF GEF-H1 is required for oncogenic RAS signaling via KSR-1. *Cancer Cell* **25**, 181–195 (2014).
27. D. Meiri, C. B. Marshall, M. A. Greeve, B. Kim, M. Balan, F. Suarez, C. Bakal, C. Wu, J. Larose, N. Fine, M. Ikura, R. Rottapel, Mechanistic insight into the microtubule and actin cytoskeleton coupling through dynein-dependent RhoGEF inhibition. *Mol. Cell* **45**, 642–655 (2012).
28. D. Meiri, M. A. Greeve, A. Brunet, D. Finan, C. D. Wells, J. LaRose, R. Rottapel, Modulation of Rho guanine exchange factor Lfc activity by protein kinase A-mediated phosphorylation. *Mol. Cell. Biol.* **29**, 5963–5973 (2009).
29. F. T. Zenke, M. Krendel, C. DerMardirossian, C. C. King, B. P. Bohl, G. M. Bokoch, p21-activated kinase 1 phosphorylates and regulates 14-3-3 binding to GEF-H1, a microtubule-localized Rho exchange factor. *J. Biol. Chem.* **279**, 18392–18400 (2004).
30. D. Meiri, C. B. Marshall, D. Mokady, J. LaRose, M. Mullin, A.-C. Gingras, M. Ikura, R. Rottapel, Mechanistic insight into GPCR-mediated activation of the microtubule-associated RhoA exchange factor GEF-H1. *Nat. Commun.* **5**, 4857 (2014).
31. K. J. Roux, D. I. Kim, M. Raida, B. Burke, A promiscuous biotin ligase fusion protein identifies proximal and interacting proteins in mammalian cells. *J. Cell Biol.* **196**, 801–810 (2012).
32. D. Comartin, G. D. Gupta, E. Fussner, E. Coyaud, M. Hasegan, M. Archinti, S. W. T. Cheung, D. Pinchev, S. Lawo, B. Raught, D. P. Bazett-Jones, J. Lüders, L. Pelletier, CEP120 and SPICE1 cooperate with CPAP in centriole elongation. *Curr. Biol.* **23**, 1360–1366 (2013).
33. M. G. Callow, S. Zozulya, M. L. Gishizky, B. Jallal, T. Smeal, PAK4 mediates morphological changes through the regulation of GEF-H1. *J. Cell Sci.* **118**, 1861–1872 (2005).
34. G. D. Gupta, É. Coyaud, J. Gonçalves, B. A. Mojarad, Y. Liu, Q. Wu, L. Gheiratmand, D. Comartin, J. M. Tkach, S. W. T. Cheung, M. Bashkurov, M. Hasegan, J. D. Knight, Z.-Y. Lin, M. Schueler, F. Hildebrandt, J. Moffat, A.-C. Gingras, B. Raught, L. Pelletier, A dynamic protein interaction landscape of the human centrosome-cilium interface. *Cell* **163**, 1484–1499 (2015).
35. Y. Yoshimura, H. Miki, Dynamic regulation of GEF-H1 localization at microtubules by Par1b/MARK2. *Biochem. Biophys. Res. Commun.* **408**, 322–328 (2011).
36. Y. Yamahashi, Y. Saito, N. Murata-Kamiya, M. Hatakeyama, Polarity-regulating kinase partitioning-defective 1b (PAR1b) phosphorylates guanine nucleotide exchange factor H1 (GEF-H1) to regulate RhoA-dependent actin cytoskeletal reorganization. *J. Biol. Chem.* **286**, 44576–44584 (2011).
37. A. L. Couzens, J. D. R. Knight, M. J. Kean, G. Teo, A. Weiss, W. H. Dunham, Z.-Y. Lin, R. D. Bagshaw, F. Sicheri, T. Pawson, J. L. Wrana, H. Choi, A.-C. Gingras, Protein interaction network of the mammalian Hippo pathway reveals mechanisms of kinase-phosphatase interactions. *Sci. Signal.* **6**, rs15 (2013).
38. D. Bhandari, J. Zhang, S. Menon, C. Lord, S. Chen, J. R. Helm, K. Thorsen, K. D. Corbett, J. C. Hay, S. Ferro-Novick, Sit4p/PP6 regulates ER-to-Golgi traffic by controlling the dephosphorylation of COPII coat subunits. *Mol. Biol. Cell* **24**, 2727–2738 (2013).
39. S. Ogg, B. Gabrielli, H. Piwnica-Worms, Purification of a serine kinase that associates with and phosphorylates human Cdc25C on serine 216. *J. Biol. Chem.* **269**, 30461–30469 (1994).
40. J. Müller, D. A. Ritt, T. D. Copeland, D. K. Morrison, Functional analysis of C-TAK1 substrate binding and identification of PKP2 as a new C-TAK1 substrate. *EMBO J.* **22**, 4431–4442 (2003).
41. J. Lim, M. Zhou, T. D. Veenstra, D. K. Morrison, The CNK1 scaffold binds cytohesins and promotes insulin pathway signaling. *Genes Dev.* **24**, 1496–1506 (2010).
42. S. Dale, W. A. Wilson, A. M. Edelman, D. G. Hardie, Similar substrate recognition motifs for mammalian AMP-activated protein kinase, higher plant HMG-CoA reductase kinase-A, yeast SNF1, and mammalian calmodulin-dependent protein kinase I. *FEBS Lett.* **361**, 191–195 (1995).
43. J. E. Hutti, E. T. Jarrell, J. D. Chang, D. W. Abbott, P. Storz, A. Toker, L. C. Cantley, B. E. Turk, A rapid method for determining protein kinase phosphorylation specificity. *Nat. Methods* **1**, 27–29 (2004).
44. P. Riou, S. Kjær, R. Garg, A. Purkiss, R. George, R. J. Cain, G. Bineva, N. Reymond, B. McColl, A. J. Thompson, N. O'Reilly, N. Q. McDonald, P. J. Parker, A. J. Ridley, 14-3-3 proteins interact with a hybrid prenyl-phosphorylation motif to inhibit G proteins. *Cell* **153**, 640–653 (2013).
45. T. Obsil, V. Obsilova, Structural basis of 14-3-3 protein functions. *Semin. Cell Dev. Biol.* **22**, 663–672 (2011).
46. C. B. Marshall, D. Meiri, M. J. Smith, M. T. Mazhab-Jafari, G. M. C. Gasmi-Seabrook, R. Rottapel, V. Stambolic, M. Ikura, Probing the GTPase cycle with real-time NMR: GAP and GEF activities in cell extracts. *Methods* **57**, 473–485 (2012).
47. N. Kobayashi, S. M. V. Freund, J. Chatellier, R. Zahn, A. R. Fersht, NMR analysis of the binding of a rhodanese peptide to a minichaperone in solution. *J. Mol. Biol.* **292**, 181–190 (1999).
48. A. W. E. Chan, E. G. Hutchinson, D. Harris, J. M. Thornton, Identification, classification, and analysis of beta-bulges in proteins. *Protein Sci.* **2**, 1574–1590 (1993).
49. P. Craveur, A. P. Joseph, J. Rebehmed, A. G. de Brevern, β-Bulges: Extensive structural analyses of β-sheets irregularities. *Protein Sci.* **22**, 1366–1378 (2013).
50. J. Z. Chuang, T. Y. Yeh, F. Bollati, C. Conde, F. Canavosio, A. Caceres, C. H. Sung, The dynein light chain Tctex-1 has a dynein-independent role in actin remodeling during neurite outgrowth. *Dev. Cell* **9**, 75–86 (2005).
51. J. C. Williams, P. L. Roulhac, A. G. Roy, R. B. Vallee, M. C. Fitzgerald, W. A. Hendrickson, Structural and thermodynamic characterization of a cytoplasmic dynein light chain–intermediate chain complex. *Proc. Natl. Acad. Sci. U.S.A.* **104**, 10028–10033 (2007).
52. G. T. Cantin, W. Yi, B. Lu, S. K. Park, T. Xu, J.-D. Lee, J. R. Yates III, Combining protein-based IMAC, peptide-based IMAC, and MudPIT for efficient phosphoproteomic analysis. *J. Proteome Res.* **7**, 1346–1351 (2008).
53. N. Dephoure, C. Zhou, J. Villén, S. A. Beausoleil, C. E. Bakalarski, S. J. Elledge, S. P. Gygi, A quantitative atlas of mitotic phosphorylation. *Proc. Natl. Acad. Sci. U.S.A.* **105**, 10762–10767 (2008).
54. V. Mayya, D. H. Lundgren, S.-I. Hwang, K. Rezaul, L. Wu, J. K. Eng, V. Rodionov, D. K. Han, Quantitative phosphoproteomic analysis of T cell receptor signaling reveals system-wide modulation of protein-protein interactions. *Sci. Signal.* **2**, ra46 (2009).
55. M. Nousiainen, H. H. Silljé, G. Sauer, E. A. Nigg, R. Körner, Phosphoproteome analysis of the human mitotic spindle. *Proc. Natl. Acad. Sci. U.S.A.* **103**, 5391–5396 (2006).
56. B. E. Schaffer, R. S. Levin, N. T. Hertz, T. J. Maures, M. L. Schoof, P. E. Hollstein, B. A. Benayoun, M. R. Banko, R. J. Shaw, K. M. Shokat, A. Brunet, Identification of AMPK phosphorylation sites reveals a network of proteins involved in cell invasion and facilitates large-scale substrate prediction. *Cell Metab.* **22**, 907–921 (2015).
57. P. E. Wright, H. J. Dyson, Intrinsically disordered proteins in cellular signalling and regulation. *Nat. Rev. Mol. Cell Biol.* **16**, 18–29 (2015).
58. J. Merino-Gracia, H. Zamora-Carreras, M. Bruix, I. Rodriguez-Crespo, Molecular basis for the protein recognition specificity of the dynein light chain DYNLT1/Tctex1: Characterization of the interaction with activin receptor IIB. *J. Biol. Chem.* **291**, 20962–20975 (2016).
59. M. Balan, thesis, University of Toronto, Canada (2013).
60. S. Ory, M. Zhou, T. P. Conrads, T. D. Veenstra, D. K. Morrison, Protein phosphatase 2A positively regulates Ras signaling by dephosphorylating KSR1 and Raf-1 on critical 14-3-3 binding sites. *Curr. Biol.* **13**, 1356–1364 (2003).
61. J.-M. Sontag, V. Nunbhakdi-Craig, C. L. White III, S. Halpain, E. Sontag, The protein phosphatase PP2A/Bα binds to the microtubule-associated proteins Tau and MAP2 at a motif also recognized by the kinase Fyn: Implications for tauopathies. *J. Biol. Chem.* **287**, 14984–14993 (2012).
62. G. R. Watkins, N. Wang, M. D. Mazalouskas, R. J. Gomez, C. R. Guthrie, B. C. Kraemer, S. Schweiger, B. W. Spiller, B. E. Wadzinski, Monoubiquitination promotes calpain

cleavage of the protein phosphatase 2A (PP2A) regulatory subunit α4, altering PP2A stability and microtubule-associated protein phosphorylation. *J. Biol. Chem.* **287**, 24207–24215 (2012).
63. J. M. Lizcano, O. Göransson, R. Toth, M. Deak, N. A. Morrice, J. Boudeau, S. A. Hawley, L. Udd, T. P. Mäkelä, D. G. Hardie, D. R. Alessi, LKB1 is a master kinase that activates 13 kinases of the AMPK subfamily, including MARK/PAR-1. *EMBO J.* **23**, 833–843 (2004).
64. J.-W. Wang, Y. Imai, B. Lu, Activation of PAR-1 kinase and stimulation of tau phosphorylation by diverse signals require the tumor suppressor protein LKB1. *J. Neurosci.* **27**, 574–581 (2007).
65. O. Göransson, M. Deak, S. Wullschleger, N. A. Morrice, A. R. Prescott, D. R. Alessi, Regulation of the polarity kinases PAR-1/MARK by 14-3-3 interaction and phosphorylation. *J. Cell Sci.* **119**, 4059–4070 (2006).
66. D. E. Jenne, H. Reimann, J.-i. Nezu, W. Friedel, S. Loff, R. Jeschke, O. Müller, W. Back, M. Zimmer, Peutz-Jeghers syndrome is caused by mutations in a novel serine threonine kinase. *Nat. Genet.* **18**, 38–43 (1998).
67. A. Hemminki, D. Markie, I. Tomlinson, E. Avizienyte, S. Roth, A. Loukola, G. Bignell, W. Warren, M. Aminoff, P. Höglund, H. Jarvinen, P. Kristo, K. Pelin, M. Ridanpää, R. Salovaara, T. Toro, W. Bodmer, S. Olschwang, A. S. Olsen, M. R. Stratton, A. de la Chapelle, L. A. Aaltonen, A serine/threonine kinase gene defective in Peutz-Jeghers syndrome. *Nature* **391**, 184–187 (1998).
68. S. G. Martin, D. St Johnston, A role for *Drosophila* LKB1 in anterior–posterior axis formation and epithelial polarity. *Nature* **421**, 379–384 (2003).
69. J. L. Watts, D. G. Morton, J. Bestman, K. J. Kemphues, The *C. elegans par-4* gene encodes a putative serine-threonine kinase required for establishing embryonic asymmetry. *Development* **127**, 1467–1475 (2000).
70. A. F. Baas, J. Kuipers, N. N. van der Wel, E. Batlle, H. K. Koerten, P. J. Peters, H. C. Clevers, Complete polarization of single intestinal epithelial cells upon activation of LKB1 by STRAD. *Cell* **116**, 457–466 (2004).
71. D. B. Shackelford, E. Abt, L. Gerken, D. S. Vasquez, A. Seki, M. Leblanc, L. Wei, M. C. Fishbein, J. Czernin, P. S. Mischel, R. J. Shaw, LKB1 inactivation dictates therapeutic response of non-small cell lung cancer to the metabolism drug phenformin. *Cancer Cell* **23**, 143–158 (2013).
72. C. Y. Peng, P. R. Graves, S. Ogg, R. S. Thoma, M. J. Byrnes III, Z. Wu, M. T. Stephenson, H. Piwnica-Worms, C-TAK1 protein kinase phosphorylates human Cdc25C on serine 216 and promotes 14-3-3 protein binding. *Cell Growth Differ.* **9**, 197–208 (1998).
73. J. Müller, S. Ory, T. Copeland, H. Piwnica-Worms, D. K. Morrison, C-TAK1 regulates Ras signaling by phosphorylating the MAPK scaffold, KSR1. *Mol. Cell* **8**, 983–993 (2001).
74. M. K. Dougherty, D. K. Morrison, Unlocking the code of 14-3-3. *J. Cell Sci.* **117**, 1875–1884 (2004).
75. K. Bajaj Pahuja, J. Wang, A. Blagoveshchenskaya, L. Lim, M. S. Madhusudhan, P. Mayinger, R. Schekman, Phosphoregulatory protein 14-3-3 facilitates SAC1 transport from the endoplasmic reticulum. *Proc. Natl. Acad. Sci. U.S.A.* **112**, E3199–E3206 (2015).
76. B. Lontay, A. Kiss, P. Gergely, D. J. Hartshorne, F. Erdödi, Okadaic acid induces phosphorylation and translocation of myosin phosphatase target subunit 1 influencing myosin phosphorylation, stress fiber assembly and cell migration in HepG2 cells. *Cell. Signal.* **17**, 1265–1275 (2005).
77. Y.-C. Chang, P. Nalbant, J. Birkenfeld, Z.-F. Chang, G. M. Bokoch, GEF-H1 couples nocodazole-induced microtubule disassembly to cell contractility via RhoA. *Mol. Biol. Cell* **19**, 2147–2153 (2008).
78. N. Fine, I. D. Dimitriou, J. Rullo, M. J. Sandi, B. Petri, J. Haitsma, H. Ibrahim, J. La Rose, M. Glogauer, P. Kubes, M. Cybulsky, R. Rottapel, GEF-H1 is necessary for neutrophil shear stress–induced migration during inflammation. *J. Cell Biol.* **215**, 107–119 (2016).
79. M. Krendel, F. T. Zenke, G. M. Bokoch, Nucleotide exchange factor GEF-H1 mediates cross-talk between microtubules and the actin cytoskeleton. *Nat. Cell Biol.* **4**, 294–301 (2002).
80. H. Lavoie, M. Therrien, Regulation of RAF protein kinases in ERK signalling. *Nat. Rev. Mol. Cell Biol.* **16**, 281–298 (2015).
81. D. Matallanas, M. Birtwistle, D. Romano, A. Zebisch, J. Rauch, A. von Kriegsheim, W. Kolch, Raf family kinases: Old dogs have learned new tricks. *Genes Cancer* **2**, 232–260 (2011).
82. C. Johnson, S. Crowther, M. J. Stafford, D. G. Campbell, R. Toth, C. MacKintosh, Bioinformatic and experimental survey of 14-3-3-binding sites. *Biochem. J.* **427**, 69–78 (2010).
83. A. J. Smith, J. Daut, B. Schwappach, Membrane proteins as 14-3-3 clients in functional regulation and intracellular transport. *Phys. Chem. Chem. Phys.* **26**, 181–191 (2011).
84. M. B. Yaffe, K. Rittinger, S. Volinia, P. R. Caron, A. Aitken, H. Leffers, S. J. Gamblin, S. J. Smerdon, L. C. Cantley, The structural basis for 14-3-3:Phosphopeptide binding specificity. *Cell* **91**, 961–971 (1997).
85. S. Rajan, R. Preisig-Müller, E. Wischmeyer, R. Nehring, P. J. Hanley, V. Renigunta, B. Musset, G. Schlichthörl, C. Derst, A. Karschin, J. Daut, Interaction with 14-3-3 proteins promotes functional expression of the potassium channels TASK-1 and TASK-3. *J. Physiol.* **545**, 13–26 (2002).
86. J. C. Obenauer, L. C. Cantley, M. B. Yaffe, Scansite 2.0: Proteome-wide prediction of cell signaling interactions using short sequence motifs. *Nucleic Acids Res.* **31**, 3635–3641 (2003).
87. H. Takala, E. Nurminen, S. M. Nurmi, M. Aatonen, T. Strandin, M. Takatalo, T. Kiema, C. G. Gahmberg, J. Ylänne, S. C. Fagerholm, β2 integrin phosphorylation on Thr758 acts as a molecular switch to regulate 14-3-3 and filamin binding. *Blood* **112**, 1853–1862 (2008).
88. A. Suzuki, M. Hirata, K. Kamimura, R. Maniwa, T. Yamanaka, K. Mizuno, M. Kishikawa, H. Hirose, Y. Amano, N. Izumi, Y. Miwa, S. Ohno, aPKC acts upstream of PAR-1b in both the establishment and maintenance of mammalian epithelial polarity. *Curr. Biol.* **14**, 1425–1435 (2004).
89. F. Dequiedt, M. Martin, J. Von Blume, D. Vertommen, E. Lecomte, N. Mari, M.-F. Heinen, M. Bachmann, J.-C. Twizere, M. C. Huang, M. H. Rider, H. Piwnica-Worms, T. Seufferlein, R. Kettmann, New role for hPar-1 kinases EMK and C-TAK1 in regulating localization and activity of class IIa histone deacetylases. *Mol. Cell. Biol.* **26**, 7086–7102 (2006).
90. S. L. Pelech, Networking with proline-directed protein kinases implicated in tau phosphorylation. *Neurobiol. Aging* **16**, 247–256 (1995).
91. J. A. Ubersax, J. E. Ferrell Jr., Mechanisms of specificity in protein phosphorylation. *Nat. Rev. Mol. Cell Biol.* **8**, 530–541 (2007).
92. Y. Saito, N. Murata-Kamiya, T. Hirayama, Y. Ohba, M. Hatakeyama, Conversion of *Helicobacter pylori* CagA from senescence inducer to oncogenic driver through polarity-dependent regulation of p21. *J. Exp. Med.* **207**, 2157–2174 (2010).
93. S. Illenberger, G. Drewes, B. Trinczek, J. Biernat, H. E. Meyer, J. B. Olmsted, E. M. Mandelkow, E. Mandelkow, Phosphorylation of microtubule-associated proteins MAP2 and MAP4 by the protein kinase $p110_{mark}$. Phosphorylation sites and regulation of microtubule dynamics. *J. Biol. Chem.* **271**, 10834–10843 (1996).
94. G. Drewes, B. Trinczek, S. Illenberger, J. Biernat, G. Schmitt-UIms, H. E. Meyer, E.-M. Mandelkow, E. Mandelkow, Microtubule-associated protein/microtubule affinity-regulating kinase ($p110^{mark}$). A novel protein kinase that regulates tau-microtubule interactions and dynamic instability by phosphorylation at the Alzheimer-specific site serine 262. *J. Biol. Chem.* **270**, 7679–7688 (1995).
95. H. Lund, E. Gustafsson, A. Svensson, M. Nilsson, M. Berg, D. Sunnemark, G. von Euler, MARK4 and MARK3 associate with early tau phosphorylation in Alzheimer's disease granulovacuolar degeneration bodies. *Acta Neuropathol. Commun.* **2**, 22 (2014).
96. G. J. Gu, H. Lund, D. Wu, A. Blokzijl, C. Classon, G. von Euler, U. Landegren, D. Sunnemark, M. Kamali-Moghaddam, Role of individual MARK isoforms in phosphorylation of tau at Ser^{262} in Alzheimer's disease. *Neuromolecular Med.* **15**, 458–469 (2013).
97. S. Pietra, A. Gustavsson, C. Kiefer, L. Kalmbach, P. Hörstedt, Y. Ikeda, A. N. Stepanova, J. M. Alonso, M. Grebe, *Arabidopsis SABRE* and *CLASP* interact to stabilize cell division plane orientation and planar polarity. *Nat. Commun.* **4**, 2779 (2013).
98. K. Itoh, O. Ossipova, S. Y. Sokol, GEF-H1 functions in apical constriction and cell intercalations and is essential for vertebrate neural tube closure. *J. Cell Sci.* **127**, 2542–2553 (2014).
99. A. Raya-Sandino, A. Castillo-Kauil, A. Dominguez-Calderon, L. Alarcon, D. Flores-Benitez, F. Cuellar-Perez, B. Lopez-Bayghen, B. Chavez-Munguia, J. Vazquez-Prado, L. Gonzalez-Mariscal, Zonula occludens-2 regulates Rho proteins activity and the development of epithelial cytoarchitecture and barrier function. *Biochim. Biophys. Acta* **1864**, 1714–1733 (2017).
100. M. Ashburner, C. A. Ball, J. A. Blake, D. Botstein, H. Butler, J. M. Cherry, A. P. Davis, K. Dolinski, S. S. Dwight, J. T. Eppig, M. A. Harris, D. P. Hill, L. Issel-Tarver, A. Kasarskis, S. Lewis, J. C. Matese, J. E. Richardson, M. Ringwald, G. M. Rubin, G. Sherlock, Gene ontology: Tool for the unification of biology. The Gene Ontology Consortium. *Nat. Genet.* **25**, 25–29 (2000).
101. Gene Ontology Consortium, Gene Ontology Consortium: Going forward. *Nucleic Acids Res.* **43**, D1049–D1056 (2015).
102. P. Shannon, A. Markiel, O. Ozier, N. S. Baliga, J. T. Wang, D. Ramage, N. Amin, B. Schwikowski, T. Ideker, Cytoscape: A software environment for integrated models of biomolecular interaction networks. *Genome Res.* **13**, 2498–2504 (2003).
103. D. Warde-Farley, S. L. Donaldson, O. Comes, K. Zuberi, R. Badrawi, P. Chao, M. Franz, C. Grouios, F. Kazi, C. T. Lopes, A. Maitland, S. Mostafavi, J. Montojo, Q. Shao, G. Wright, G. D. Bader, Q. Morris, The GeneMANIA prediction server: Biological network integration for gene prioritization and predicting gene function. *Nucleic Acids Res.* **38**, W214–W220 (2010).
104. C. J. A. Sigrist, L. Cerutti, N. Hulo, A. Gattiker, L. Falquet, M. Pagni, A. Bairoch, P. Bucher, PROSITE: A documented database using patterns and profiles as motif descriptors. *Brief. Bioinform.* **3**, 265–274 (2002).
105. E. de Castro, C. J. A. Sigrist, A. Gattiker, V. Bulliard, P. S. Langendijk-Genevaux, E. Gasteiger, A. Bairoch, N. Hulo, ScanProsite: Detection of PROSITE signature matches and ProRule-associated functional and structural residues in proteins. *Nucleic Acids Res.* **34**, W362–W365 (2006).
106. UniProt Consortium, UniProt: A hub for protein information. *Nucleic Acids Res.* **43**, D204–D212 (2015).

107. P. Bawono, J. Heringa, PRALINE: A versatile multiple sequence alignment toolkit. *Methods Mol. Biol.* **1079**, 245–262 (2014).
108. V. A. Simossis, J. Kleinjung, J. Heringa, Homology-extended sequence alignment. *Nucleic Acids Res.* **33**, 816–824 (2005).
109. D. K. Morrison, G. Heidecker, U. R. Rapp, T. D. Copeland, Identification of the major phosphorylation sites of the Raf-1 kinase. *J. Biol. Chem.* **268**, 17309–17316 (1993).
110. M. Therrien, N. R. Michaud, G. M. Rubin, D. K. Morrison, KSR modulates signal propagation within the MAPK cascade. *Genes Dev.* **10**, 2684–2695 (1996).
111. F. Delaglio, S. Grzesiek, G. W. Vuister, G. Zhu, J. Pfeifer, A. Bax, NMRPipe: A multidimensional spectral processing system based on UNIX pipes. *J. Biomol. NMR* **6**, 277–293 (1995).
112. T. Holyoak, T. D. Fenn, M. A. Wilson, A. G. Moulin, D. Ringe, G. A. Petsko, Malonate: A versatile cryoprotectant and stabilizing solution for salt-grown macromolecular crystals. *Acta Crystallogr. D Biol. Crystallogr.* **59**, 2356–2358 (2003).
113. D. Kessner, M. Chambers, R. Burke, D. Agus, P. Mallick, ProteoWizard: Open source software for rapid proteomics tools development. *Bioinformatics* **24**, 2534–2536 (2008).
114. R. Craig, R. C. Beavis, TANDEM: Matching proteins with tandem mass spectra. *Bioinformatics* **20**, 1466–1467 (2004).
115. P. G. A. Pedrioli, Trans-proteomic pipeline: A pipeline for proteomic analysis. *Methods Mol. Biol.* **604**, 213–238 (2010).
116. E. W. Deutsch, L. Mendoza, D. Shteynberg, T. Farrah, H. Lam, N. Tasman, Z. Sun, E. Nilsson, B. Pratt, B. Prazen, J. K. Eng, D. B. Martin, A. I. Nesvizhskii, R. Aebersold, A guided tour of the Trans-Proteomic Pipeline. *Proteomics* **10**, 1150–1159 (2010).
117. G. Liu, J. Zhang, B. Larsen, C. Stark, A. Breitkreutz, Z.-Y. Lin, B.-J. Breitkreutz, Y. Ding, K. Colwill, A. Pasculescu, T. Pawson, J. L. Wrana, A. I. Nesvizhskii, B. Raught, M. Tyers, A.-C. Gingras, ProHits: Integrated software for mass spectrometry–based interaction proteomics. *Nat. Biotechnol.* **28**, 1015–1017 (2010).
118. G. Teo, G. Liu, J. Zhang, A. I. Nesvizhskii, A.-C. Gingras, H. Choi, *SAINTexpress*: Improvements and additional features in Significance Analysis of INTeractome software. *J. Proteomics* **100**, 37–43 (2014).
119. H. Choi, B. Larsen, Z.-Y. Lin, A. Breitkreutz, D. Mellacheruvu, D. Fermin, Z. S. Qin, M. Tyers, A.-C. Gingras, A. I. Nesvizhskii, SAINT: Probabilistic scoring of affinity purification–mass spectrometry data. *Nat. Methods* **8**, 70–73 (2011).

Acknowledgments: We gratefully acknowledge J. Normand for technical assistance, G. Gasmi-Seabrook for assistance with NMR spectroscopy, and J. St-Germain for assistance in uploading the MS data. We also thank S. Keezer (Cell Signaling Technology) for the generation of phospho-specific antibodies used in this study, T. Moraes for the MST instrument access, and S. Muthuswamy (Beth Israel Deaconess Medical Center/Harvard Medical) and M. Zhang (Hong Kong University of Science and Technology) for providing reagents. Finally, we would like to thank M. Wagner, F. Sircoulomb, and O. Kent for helpful discussions during development of the study. **Funding:** This work was supported by the Canadian Cancer Society Research Institute grants to R.R. (CCSRI 704107) and M.I. (703209). M.I. was supported by the Cancer Research Society (CRS 14014), Princess Margaret Foundation, and Canadian Institutes for Health Research. R.R. holds the Amgen Chair for Cancer Research at the Princess Margaret Cancer Centre. M.I. holds the Canada Research Chair in Cancer Structural Biology. The NMR facility at University Health Network is supported by the Canada Foundation for Innovation. **Author contributions:** M.-J.S., C.B.M., M.I., D.K.M., and R.R. designed the study. M.-J.S., A.A.C., and J.L.R. performed the molecular biology experiments (immunoprecipitation, Western blotting, and immunofluorescence). C.B.M. performed the MST and fluorescence polarization experiments. C.B.M. and M.B. performed the NMR experiments. M.B. conducted the work related to the crystallization of the chimera under the supervision of C.B.M., N.I., and M.I.; D.K.M. did the coimmunoprecipitation, metabolic labeling, and all the phosphopeptide mapping experiments concerning MARK3. M.Z. performed the MARK3 MS analysis. D.M.M. generated (and performed) the ARHGEF2 and MARK3 mutants for the in vitro kinase assays. E.C. conducted the BioID for ARHGEF2 and MS experiments under the supervision of B.R. A.L.C. generated the different PP6 cell lines used in this study under the supervision of A.-C.G. E.C. and B.R. performed the analysis of the BioID MS raw data. M.-J.S., C.B.M., M.B., and D.K.M. performed the formal analysis of the data. W.X. supervised the statistical analysis. M.-J.S. visualized the data. M.-J.S., C.B.M., M.B., M.I., D.K.M., and R.R. wrote, reviewed, and edited the manuscript. **Competing interests:** The authors declare that they have no competing interests. **Data and materials availability:** The MS proteomic data have been deposited to MassIVE (Mass Spectrometry Interactive Virtual Environment, a member of the ProteomeXchange Consortium) (https://massive.ucsd.edu/ProteoSAFe/static/massive.jsp) with the reference numbers MassIVE MSV000081222 for ARHGEF2 and MassIVE MSV000081223 for C-TAK1 (MARK3). The crystal structure has been deposited at the PDB (www.rcsb.org/pdb/) (PDB: 5WI4). Plasmids require a material transfer agreement from the University Health Network Technology Development and Commercialization Office.

Submitted 30 March 2017
Accepted 6 October 2017
Published 31 October 2017
10.1126/scisignal.aan3286

Citation: M.-J. Sandí, C. B. Marshall, M. Balan, É. Coyaud, M. Zhou, D. M. Monson, N. Ishiyama, A. A. Chandrakumar, J. La Rose, A. L. Couzens, A.-C. Gingras, B. Raught, W. Xu, M. Ikura, D. K. Morrison, R. Rottapel, MARK3-mediated phosphorylation of ARHGEF2 couples microtubules to the actin cytoskeleton to establish cell polarity. *Sci. Signal.* **10**, eaan3286 (2017).

Science Signaling

MARK3-mediated phosphorylation of ARHGEF2 couples microtubules to the actin cytoskeleton to establish cell polarity

María-José Sandí, Christopher B. Marshall, Marc Balan, Étienne Coyaud, Ming Zhou, Daniel M. Monson, Noboru Ishiyama, Arun A. Chandrakumar, José La Rose, Amber L. Couzens, Anne-Claude Gingras, Brian Raught, Wei Xu, Mitsuhiko Ikura, Deborah K. Morrison and Robert Rottapel

Sci. Signal. **10** (503), eaan3286.
DOI: 10.1126/scisignal.aan3286

MARKing the switch from microtubules to actin

To enable them to carry out specialized functions, many cell types become polarized through the activity of various proteins, including the kinases of the MARK family. Sandí *et al*. found that MARK3 phosphorylated Ser^{151} in the cytoskeleton-associated protein ARHGEF2. This phosphorylation event caused ARHGEF2 to dissociate from microtubules and activate RHOA, resulting in the formation of focal adhesions and stress fibers and enabling the formation of three-dimensional structures by cultured cells. These effects were reversed by the PP2A-mediated dephosphorylation of Ser^{151} in ARHGEF2. Thus, the phosphorylation state of Ser^{151} of ARHGEF2 determines whether it is sequestered by the tubulin cytoskeleton or released to remodel the actin cytoskeleton and regulate cell polarity.